Article

Newly Synthesized Anticancer Purine Derivatives Inhibiting *p*-EIF4E Using Surface-Modified Lipid Nanovesicles

Reem T. Attia, Menna A. Ewida, Eman Khaled, Sherif Ashraf Fahmy,* and Iten M. Fawzy*

Read Online

ACCESS | 📊 Metrics & More | 📖 Article Recommendations | 🆘 Supporting Information

ABSTRACT: Translation of mRNA is one of the processes adopted by cancer cells to maintain survival via phosphorylated (*p*)-eIF4E overexpression. Once *p*-eIF4E binds to the cap structure of mRNA, it advocates a nonstop translation process. In this regard, 15 new-based GMP analogs were synthesized to target eIF4E and restrain its binding to cap mRNA. The compounds were tested against three types of cancer cell lines: Caco-2, HepG-2, MCF-7, and normal kidney cells (Vero cells). Most of the compounds showed high potency against breast cancer cells (MCF-7), characterized by the highest cancer type for overexpression of *p*-eIF4E. Compound **4b** was found to be the most active against three cell lines, colon (Caco-2), hepatic (HepG-2), and breast (MCF-7), with positive IC_{50} values of 31.40, 27.15, and 21.71 μM, respectively. Then, chitosan-coated niosomes loaded with compound **4b** (Cs/**4b**-NSs) were developed (as kinetically enhanced molecules) to improve the anticancer effects further. The prepared Cs/**4b**-NSs showed pronounced cytotoxicity compared to the free **4b** against Caco2, Hepg2, and MCF-7 with IC_{50} values of 16.15, 26.66, and 6.90 μM, respectively. Then, the expression of both the phosphorylated and nonphosphorylated western blot techniques was conducted on MCF-7 cells treated with the most active compounds (based on the obtained IC_{50} values) to determine the total protein expression of both eIF4E and *p*-eIF4e. Interestingly, the selected most active compounds displayed 35.8−40.7% inhibition of *p*-eIF4E expression when evaluated on MCF-7 compared to Ribavirin (positive control). CS/**4b**-NSs showed the best inhibition (40.7%). The findings of the present joint *in silico* molecular docking, simulation dynamic studies, and experimental investigation suggest the potential use of niosomal nanovesicles as a promising nanocarrier for the targeted delivery of the newly synthesized compound **4b** to eukaryotic initiation factor 4E. These outcomes support the possible use of Cs/**4b**-NSs in targeted cancer therapy.
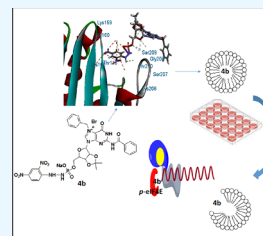
1. INTRODUCTION

Messenger RNA (mRNA) translation is the most energy-intensive process in a cell and is considered crucial for controlling gene expression.[1−3] The initiation of translation is controlled by the eukaryotic initiation factor 4F (eIF4F) complex. It consists of the ATP-dependent RNA helicase eIF4A, the large scaffolding protein eIF4G, and the 5′ mRNA cap-binding subunit eIF4E. The recognition of the 7-methylguanosine nucleoside triphosphate (m7GpppX) cap at the 5′-terminus of mRNA by eIF4E is essential for initiating cap-dependent translation. Dysregulation of cap-dependent translation is linked to the development and progression of cancer.[4−6]

The availability of eIF4E is tightly controlled under typical physiological circumstances.[7] eIF4E-binding protein 1 (4EBP1) is the primary regulator of eIF4E availability and a substrate of the mechanistic target of the rapamycin (mTOR) signaling pathway.[8−11] To prevent the formation of the translation initiation complex in the dephosphorylated state, 4EBP1 and eIF4G compete for eIF4E's binding (Figure 1). When eIF4E is phosphorylated by upstream signals, primarily mTOR complex 1 (mTORC1), it is released and triggers the synthesis of several proteins, including oncogenic proteins.[12,13] However, a recently characterized downstream pathway of MAP kinase-activated protein kinase (MAPKAPK) was also shown to phosphorylate eIF4E on Ser209 via phosphorylation

of Mnk1/2 activated by Erk1, Erk2, and p38 MAP kinases released by MAPK.[14] It has been demonstrated that phosphorylated eIF4E (*p*-eIF4E) is overexpressed in numerous malignancies and is essential for cancer cell invasion and tumorigenesis.[15−18]

Developing bioavailable analogs of the 5′-cap targeting eIF4E has emerged as a crucial strategy for developing targeted anticancer agents.[19,20] Previous studies reported that mimicking the mRNA cap structure, 7-methyl guanosine (m7G) analogs compete with eIF4E for binding and thus lowering the rate of translation initiation.[21] A major antiviral medication, guanosine ribonucleoside analog Ribavirin, was initially identified as a cap-mimetic[22] and demonstrated promising results in many cancer models, including breast and ovarian cancers.[23]

Reported analogs as 7-methyl guanosine triphosphate (m7GTP)-derived nucleoside and nucleotide were tested as potential agents for controlling translation initiation generally
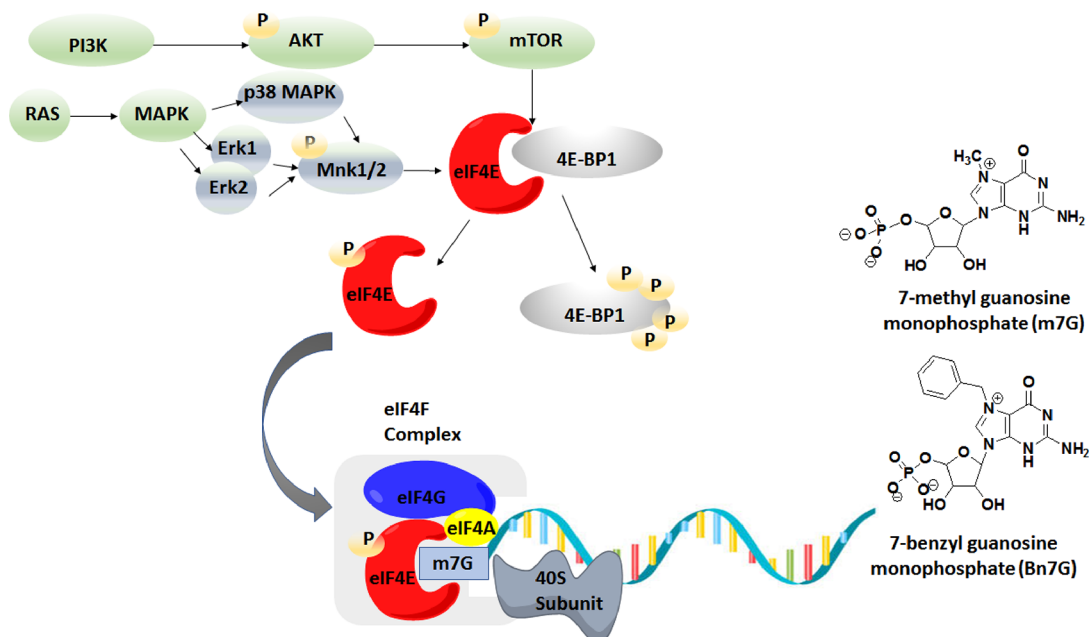
Figure 1. Cellular mechanism of translation initiation.
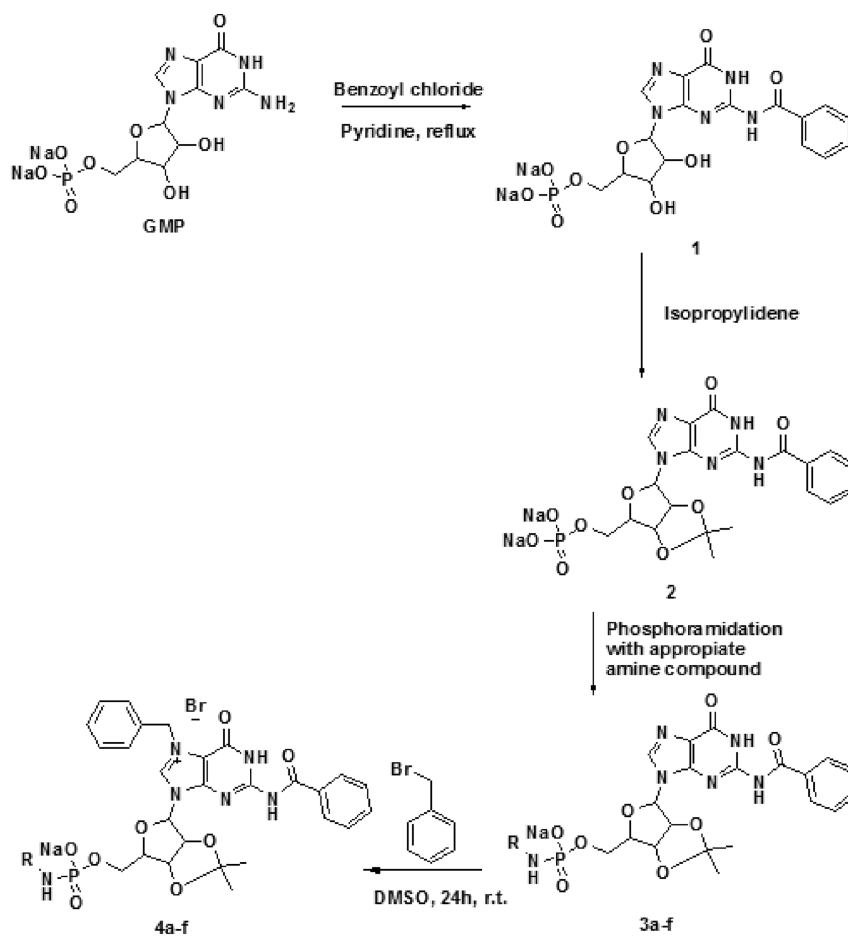
R: B-alanine, 2,4 dinitrophenyl hydrazine, *P*-*N*-ethylmorpholino aniline, *P*-*N*-phenylpiperazinyl aniline, 2-amino thiazole, 2-amino-4-(p-tolyl) thiazole

Figure 2. Scheme diagram depicting the synthesis of the new chemical compounds.
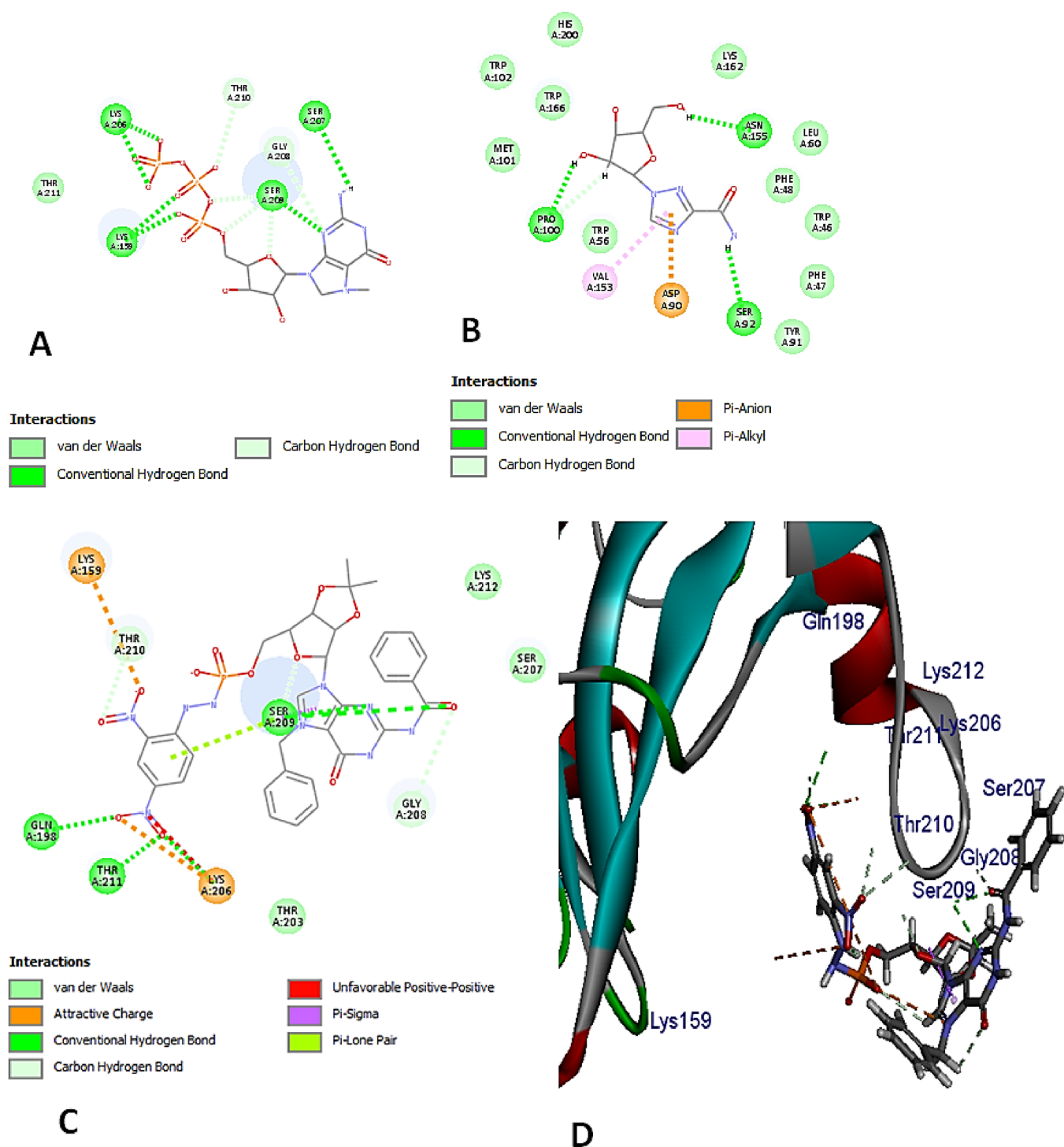
Figure 3. Docking interaction between eIf4E (3U7X) and different ligands: (A) 2D binding mode of m7GTP, (B) 2D binding mode of Ribavirin, (C) 2D binding mode of **4b**, and (D) 3D binding mode of **4b**. Blue color ribbons represent beta sheets, red color ribbons represent helix, gray color ribbons represent turns, and green color ribbons represent residues less than 10 Å.

and eIF4E binding to capped mRNA specifically. These analogs adopted alterations to the guanine moiety's N7 and N2 positions, the 5-phosphate moiety, and the ribose ring.[24,25]

On the other hand, previous studies have focused on using the synthetic nucleotide derivative 7-benzyl guanosine monophosphate (Bn7GMP) to block the binding of eIF4E to the mRNA cap since aryl substitution at N7 has shown an increased binding affinity.[24,25]

Cap analogs have been employed in studies involving the eIF4E function performed *in vitro*, but they have poor permeability and stability when used *in vivo*.[26] Prodrugs with favorable pharmacokinetic properties have been developed to overcome this challenge.[27,28]

In this study, 15 novel compounds have been designed and synthesized as small molecule analogs of the guanosine monophosphate (GMP) moiety via different phosphoramidated linkers. The new compounds were subjected to *in silico*
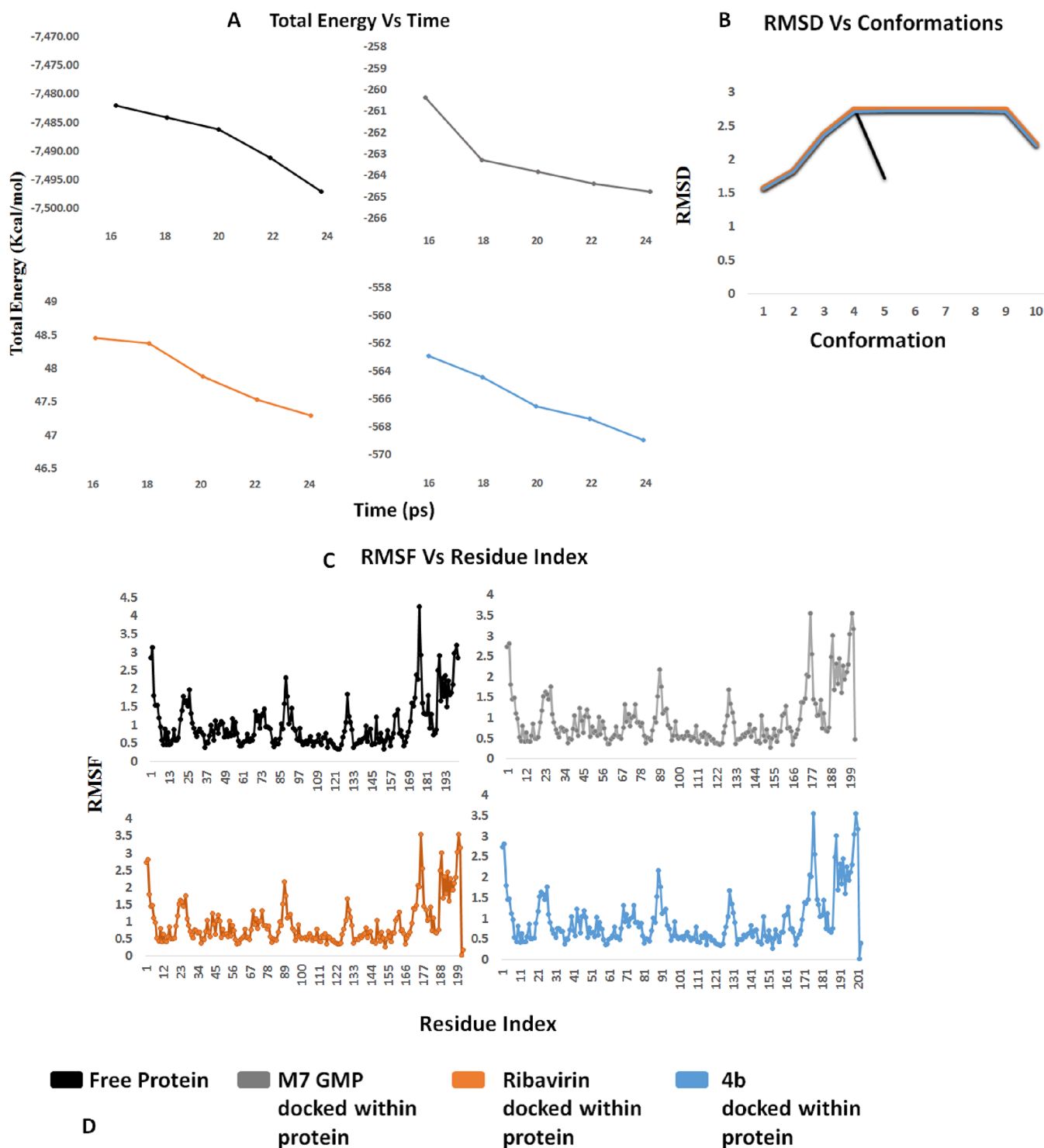
Figure 4. Results of dynamic simulation studies: (A) total energy vs time, (B) RMSD vs conformations, and (C) RMSF vs residue index. (D) Color map.

molecular docking and simulation dynamic studies against eIF4E to investigate the suspected inhibitory binding mode and expected stability over time. Moreover, ADMET and toxicity prediction studies were performed to study the pharmacokinetic properties of the newly synthesized molecules. Then, the most therapeutically active compound was encapsulated into chitosan-coated niosomes (Cs/4b-NSs) to further enhance the chemotherapeutic activity. The anti-proliferative assay was performed for the 15 molecules and Cs/

4b-NSs against three different cell lines: colon (Caco2), hepatic (HepG2), and breast (MCF-7). Then, a mechanism study was carried out using the western blot technique to measure the total protein expression in MCF-7 treated cells of both eIF4E and *p*-eIF4E.

2. RESULTS AND DISCUSSION

2.1. Chemistry. To mimic the m7G cap of the RNA and adopt strategies of structure modifications reported in the

Ramachandran Plot

A: Free Protein   **B: Protein after docking**

🟩 Favorable area   🟥 Unfavorable area   🟪 Area outside binding site   🟦 Area inside binding site
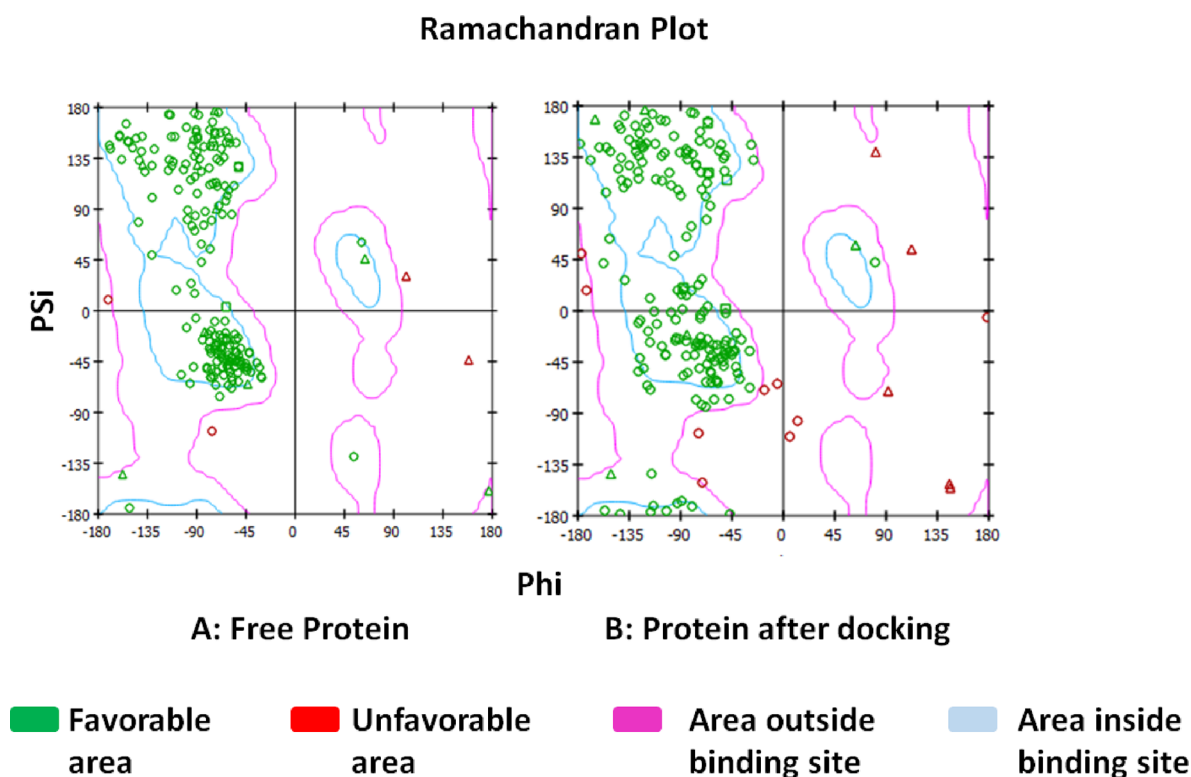
Figure 5. Ramachandran plot representation of torsional energy conformations for the interaction between **4b** and eIF4E.

literature, a guanosine nucleus was rendered, while the free amino group was modified via an amide linker through a reaction with benzoyl chloride[29] to yield benzyl amide derivatives (Figure 2). Next, the OH groups of the ribose sugar moiety were cross-linked via isopropylidene reaction.[30] As previously reported, phosphoramidation[19] of **2** was carried out using appropriate amines to produce **3a–3f**. Finally, the insertion of the benzyl group essential for activity at the N-7 atom through reaction with benzyl bromide[27] yielded **4a–4f**.

2.2. Molecular Modeling. The *in silico* molecular docking, dynamic simulation, ADMET, and toxicity studies were performed using Discovery Studio 4.0 software.

2.2.1. Molecular Docking. Based on the literature,[14] the human eIF4E bound to 4EBP can alter the attachment of inhibitors than the free protein; thus, a bound protein form was utilized to perform molecular modeling studies. A bound protein form was utilized; the crystallographic sequence of the human eIF4E-4EBP1 peptide complex[31] was downloaded from PDB: 3U7X. The novel prepared compounds (**1**, **2**, **3a–3f**, and **4a–4f**) were docked together with Bn 7G, GMP, and Ribavirin as reference drugs and m7G as the reference complexed cap ligand. Adopting the C-Docker protocol, m7G (normal cap-binding) showed an interaction energy of −31.2173 kcal/mol through phosphorylation of Ser 209 via multiple H-bonds between the target amino acid and the N atom of the guanosine ring, the O atom of the tetrahydrofuran ring, and the O atoms of phosphate groups. Also, this phosphorylation process was stacked via H-bonds with Lys 159 and Lys 206. Bn7G showed −27.2655 kcal/mol binding affinity with only a single H-bond between its *O*-tetrahydrofuran and Ser 209. Meanwhile, Ribavirin showed an interaction energy of −29.0744 kcal/mol but with docking poses away from the target site of Ser 209. The new compounds showed comparable binding affinity in a range of −(54.0213–

17.4872) kcal/mol and correct targeting to block the phosphorylation of Ser 209. Superiority was displayed by compound **4b**, hence the best interaction energy and perfect block for Ser 209 via comparable habit to that of m7G. It showed two H-bonds between the O atom of tetrahydrofuran and that of carbonyl of benzoyl amide linkage and Ser 209. Additionally, a pi-lone pair interaction between the phenyl ring of attached amine and Ser 209 thus prevented the interaction between O atoms of phosphate groups and the key amino acid Ser 209, blocking its phosphorylation. Moreover, the process was sacked through its twin nitro groups through pi-bonds with both Lys 159 and Lys 206, as shown in Figure 3. From the above results, we can conclude that **4b** could be a competitive inhibitor model.

2.2.2. Dynamic Simulations. Dynamic simulation studies and trajectory analysis were performed to prove the stability of the interaction between **4b** and eIF4E compared to reference Ribavirin and natural cap m7G.[32] Figure 4 shows the total energy versus time range of 16−24 ps of free protein expressed as −(7480−7500) kcal/mol. After interaction of **4b** with eIF4E, its dynamic simulation revealed a total energy of −(563−570) kcal/mol, a more stable and preferred mode than the complex of m7G-eIF4E, which showed −(260−266) kcal/mol or the least stable complex of Ribavirin-eIF4E, which displayed a positive unpreferrable energy of 48.5−46.5 kcal/mol. The docked complex's root-mean-square deviation (RMSD) of the three competitors was similar to no notable deviation. In addition, the root-mean-square fluctuations (RMSFs) were calculated for each residue index to evaluate flexibility, which showed strict binding and inhibition of eIF4E along most of the produced residue indices of **4b** that did not exceed 3.5. The stability was enhanced compared to the fluctuations of the free protein or the attached m7G that exceeded the allowed range of 3.5.

Table 1. ADMET Study Results of Novel Compounds and Ribavirin

compound	ADMET solubility	blood−brain barrier (BBB)	hepatotoxic prediction	expected hepatotoxicity	absorption	plasma protein binding (PPB)
Ribavirin	5	4	1.14	true	3	false
guanosine monophosphate (GMP)	4	4	3.12	true	3	false
1	3	4	4.42	true	3	false
2	3	4	3.00	true	3	false
3a	4	4	−0.91	true	3	false
3b	2	4	4.40	true	3	false
3c	3	4	−0.018	true	3	false
3d	3	4	1.74	true	3	false
3e	2	4	2.45	true	3	false
3f	2	4	2.06	true	3	false
4a	3	4	−6.19	false	3	false
4b	2	4	−1.03	true	3	false
4c	4	4	−4.88	false	3	false
4d	3	4	−3.62	true	3	false
4e	2	4	−3.29	true	3	false
4f	2	4	−3.07	true	3	false

2.2.3. Ramachandran Plot. Verification of predicted torsion angles within the target protein could be obtained by performing a Ramachandran plot. It was carried out using Discovery Studio 4.0 before and after docking to confirm the interaction of the promising compound **4b** in correct binding sites and reveal the topological changes applied to protein because ligand occupancy of the cap-binding site induces significant structural changes in eIF4E.[33] The conventional terms used to represent the torsion angles on either side of the φ carbons in peptides could be represented by low energy conformations for φ (phi) and ψ (psi). The graphical representation of Figure 5 displayed a high increase in favorable green areas during interaction with **4b** than the free protein compared to the slight increase in the red unfavorable areas and, thus, ease of multiple conformations within the binding sites of the protein.

2.2.4. ADMET Study. In silico ADMET study was performed using Discovery Studio 4.0.[34] The properties of the compounds were compared to those of reference Ribavirin (Table 1). The BBB penetration is very low among all compounds (stage 4), which reflects expectedly low undesired side effects. Some hepatotoxicity is predicted for most of the compounds but with a low probability, except for **4a** and **4c**. All compounds showed no binding to plasma proteins, which reflects expectedly lower side effects. All compounds showed very poor intestinal absorption, similar to Ribavirin, since these drugs depend on intestinal absorption via an active concentration gradient rather than normal diffusion; hence, nanoformulation was proposed as an endowed method to enhance the pharmacokinetic properties of the promising molecule.

2.2.5. TOPKAT Toxicity Study. TOPKAT Ames toxicity protocol was adopted to be applied for all novel compounds and Ribavirin to evaluate possible toxicities. All TOPKAT Ames probabilities, applications, and scores showed that compounds are neither nonmutagenic nor carcinogenic and within expected ranges (Table 2).

2.3. Chitosan-Coated Niosomal Formulation. Current chemotherapeutics delivery approaches include various nanocarriers, including metallic nanoparticles,[35] polymeric nanoparticles,[36−38] macromolecules,[39,40] silica nanoparticles,[41] and nanovesicles.[42,43] Nanovesicles (liposomes and niosomes) are lipid-based nanocarriers that are reported to encapsulate natural and synthetic chemotherapeutics, enhancing their hydrophilicity and therapeutic effects.[44] Liposomes are formed mainly of phospholipids (such as phosphatidylcholine and phosphatidylethanolamine) self-assembled in an aqueous medium, developing lipid bilayer nanovesicles.[45] On the other hand, niosomes have emerged as a reliable and modern alternative nanocarrier to liposomes. They are composed mainly of cholesterol and non-ionic surfactants engineered by self-assembly in an aqueous phase, generating bilayer vesicles.[46] Niosomes have attractive properties making them one of the promising nanovesicles in cancer therapy, such as being stable, biocompatible, biodegradable, and safe carriers with minimum immunogenic effects.[45,46] In addition, the negatively charged niosomes could be coated with the polycationic chitosan via an electrostatic interaction. Chitosan is a biocompatible and biodegradable natural polymer with mucoadhesive properties. This would lead to the adhesion of the niosomes to the cancer cell membrane, prolong the residence time of the niosomes at the site of action, and achieve a controlled release of the payload at cancer cells.[47] Thus, to exploit the benefits of loading anticancer drugs in chitosan-coated niosomes (Cs/NSs), compound **4b** was loaded into Cs/NSs, forming Cs/**4b**-NSs. Then, the designed niosomal formulation was characterized in terms of size, polydispersity index, surface charge, and shape, as shown below. Also, the entrapment efficiency and release behavior of the loaded **4b** out of the niosomal formulation were investigated.

2.3.1. Particle Size, Polydispersity Index (PDI), Zeta Potential, and Entrapment Efficiency Percentage (EE%). The particle size and PDI of the nonchitosan-coated and chitosan-coated niosomes were investigated using dynamic light scattering, and the findings are summarized in Table 3. All fabricated niosomes were found to be homogeneous (PDI < 0.3) with sizes ranging from 55 to 140 nm, enabling the drugs' passive accumulation into cancer cells, characterized by permeable vasculature and reduced lymphatic drainage.[47,48] Moreover, coating plain niosomes (NSs) and **4b**-NSs with chitosan increased the particle sizes of the chitosan-coated niosomes (98.35 ± 16.66 and 139.74 ± 64.80 nm for plain Cs/NSs and Cs/**4b**-NSs, respectively) as compared to the

Table 2. TOPKAT Ames Toxicity Study Results of Novel Compounds and Ribavirin[a]

compd	Ames pred.	Ames appl.	Ames prob.	Ames score	mouse female *NTP pred.	mouse female NTP prob.	mouse male NTP pred.	mouse male NTP prob.	rat female NTP pred.	rat female NTP prob.	rat male NTP pred.	rat male NTP prob.	carcinogenic potency **TD50 mouse (mg kg−1 day−1)	carcinogenic potency TD50 rat (mg kg−1 day−1)	rat oral ***LD50 (g/kg)	rat max. tol. dose (g/kg)
ribavirin	NM	All properties and ****OPS component are within expected ranges.	0.3	−11.79	NC	0.41	NC	0.26	NC	0.44	NC	0.52	13.11	16.62	0.75	0.15
GMP			7.67	−41.60		0.55		0.26		0.47		0.61	27.30	0.19	2.26	0.03
1			0.005	−26.88		0.44		0.31		0.50		0.53	46.22	0.41	1.17	0.03
2			0.01	−23.83		0.54		0.42		0.55		0.53	14.31	2.35	3.08	0.009
3a			0.01	−23.14		0.42		0.20		0.51		0.38	22.43	11.54	8.52	0.01
3b			0.11	−16.66		0.04		0.13		0.61		0.47	6.18	0.82	4.84	0.01
3c			0.08	−24.61		0.43		0.28		0.51		0.45	1.69	0.74	23.28	0.01
3d			0.13	−17.88		0.37		0.52		0.56		0.53	0.55	0.25	10.34	0.009
3e			0.30	−19.05		0.52		0.16		0.52		0.48	5.87	0.98	11.45	0.01
3f			0.06	−15.98		0.36		0.27		0.55		0.56	1.27	0.05	16.10	0.009
4a			0.05	−17.93		0.40		0.36		0.53		0.39	4.31	3.52	4.17	0.01
4b			0.08	−11.78		0.02		0.17		0.63		0.47	1.16	0.24	1.98	0.01
4c			0.23	−19.62		0.42		0.36		0.52		0.45	0.47	0.22	11.79	0.01
4d			0.32	−13.38		0.29		0.54		0.56		0.51	0.10	0.07	4.92	0.008
4e				−14.44		0.45		0.24		0.54		0.46	1.12	0.29	5.80	0.011
4f			0.18	−11.28		0.27		0.33		0.54		0.56	0.24	0.01	6.63	0.008

[a]Abbreviations: compd, compound; pred, prediction; appl, application; prob, probability; mg kg−1 day−1, milligrams per kilogram of body weight per day; max, maximum; tol, tolerated; NM, nonmutagen; NC, noncarcinogen.

Table 3. Particle Size, PDI, Zeta Potential, and EE% of Non-Chitosan-Coated and Chitosan-Coated L1-NSs[a]

sample	particle size (nm)	PDI	zeta potential (mV)	EE%
plain NSs	67.48 ± 10.84	0.23 ± 0.10	−3.38 ± 0.53	
plain Cs/NSs	98.35 ± 16.66	0.24 ± 0.12	+7.65 ± 0.64	
4b-NSs	55.52 ± 6.31	0.26 ± 0.27	−6.47 ± 1.07	70.3%
Cs/4b-NSs	139.74 ± 64.80	0.25 ± 0.13	+13.99 ± 0.67	90.4%

[a]All measurements were conducted in triplicate, and the results were expressed as means ± standard deviations.

noncoated niosomes (67.48 ± 10.84 and 55.52 ± 6.31 nm for plain NSs and 4b-NSs, respectively).

Likewise, the surface charge has increased after coating with chitosan from −3.38 ± 0.53 and −6.47 ± 1.07 mV (in the case of plain NSs and 4b-NSs, respectively) to +7.65 ± 0.64 and +13.99 ± 0.67 mV (in the case of plain Cs/NSs and Cs/4b-NSs, respectively). This is attributed to the presence of the cationic amino groups of chitosan on the surface, which shield the negative charges of the niosomes. These findings proved the successful coating of niosomes with chitosan.[47] The outstanding positive charge on the surface of Cs/4b-NSs hinders the clumping of the niosomal formulation upon storage. Also, it enables the adhesion of the niosomal formulation to the cancer cell membrane.[48] On the other hand, the EE% of 4b had increased from 70.3%, in the case of 4b-NSs, to 90.4%, in the case of Cs/4b-NSs, owing to reduction of the drug leakage upon coating with chitosan.[49−52] Since the Cs/4b-NSs formula exhibited a higher zeta potential and EE% than 4b-NSs, it was selected for further studies.

2.3.2. Morphological Features of Cs/4b-NSs. The morphological features of Cs/4b-NSs were studied by using TEM analysis (Figure 6A) and showed the successful construction of spherical chitosan-coated niosomes with smooth surfaces. The self-assembly of cholesterol and non-ionic surfactants can yield spherical nanovesicles in aqueous media. The unique structure of niosomes allows for the solubilization of 4b in the outer hydrophobic bilayer.

2.3.3. In Vitro Release Percentage (%). The release of 4b from Cs/4b-NSs was evaluated under physiological conditions and at cancer cells' microenvironments (pH 7.4 and pH 5.5, respectively), as illustrated in Figure 6B. The % released 4b was quantified using UV−vis spectroscopy at 250 nm. As anticipated from zeta potential measurements, Cs/4b-NSs

nanovesicles displayed outstanding stability at the physiological pH, with about 59.7% of the loaded 4b released after 48 h at 37 °C. At the cancer cell's pH, about 92% of the entrapped 4b was released after 48 h at 37 °C. These findings suggest the ability of the designed chitosan-coated niosomes to release their payload preferentially by a pH-dependent modality at tumor cells and ultimately enhance the anticancer efficiency of the fabricated nanovesicles against cancer cells.

2.4. Antiproliferative Assay. The antiproliferative activities of newly synthesized compounds (1, 2, 3a−3f, and 4a−4f), as well as two reference drugs rapamycin and Ribavirin, were tested against colorectal adenocarcinoma (Caco-2), hepatocellular carcinoma cells (HepG-2), and breast carcinoma cells (MCF-7) using sulforhodamine-B (SRB) assay.[53]

The observed results (Table 4 and Figure 7A−D) showed that most of the synthesized compounds showed high cytotoxic properties, especially against the MCF-7 cell line. This might be explained by the fact that eIF4E is overexpressed in breast cancer cells as mentioned previously.[54] Furthermore, the synthetic drugs were tested on normal kidney cells (Vero cells), and they showed minimal signs of cytotoxicity. This goes in line with previous research suggesting that targeting eIF4E preferentially inhibits the translation of oncogenic mRNAs while sparing normal mRNA translation, suggesting a degree of selectivity.[55] All series of compounds exhibited the most potent activity against MCF-7 cells, showing IC$_{50}$ in the range from 6.27 to 74.76 μM. On the other hand, series 4 compounds showed better activity against the other two cell lines, Caco-2 and HepG-2, than the rest of the compounds owing to the highest binding affinity of the N7 benzyl group. Interestingly, it was found that β-alanine and dinitrophenyl hydrazine phosphoramidated compounds showed the best activity compared to those of other peers. The ethyl-morpholino derivatives were better in cytotoxicity than the phenyl piperazines. In addition, the p-tolyl thiazole derivatives were better in cell killing than thiazoles. One of the most active compounds against HepG-2 and MCF-7 cancer cells was 4b (Figure 7B). It showed a 1.3-fold increase in cytotoxicity compared to the control drug Ribavirin and 75.1% more cytotoxicity than the control drug rapamycin in the case of the HepG-2 cell lines. The IC$_{50}$ values of compound 4b were 31.40, 27.15, and 21.71 μM against Caco-2, HepG-2, and MCF-7 cells, respectively. Afterward, compound 4b was loaded into chitosan-coated niosomal formulation (Cs/4b-NSs) and a remarkable enhancement in the cytotoxicity with 48.5, 1.8, and
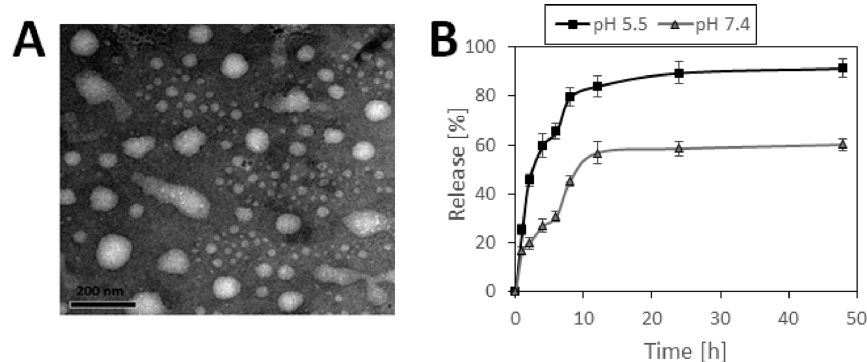
Figure 6. (A) TEM image for Cs/4b-NSs and (B) time-dependent release % of 4b from Cs/4b-NSs at 37 °C into pH 5.5 (triangle) and pH 7.4 (square).

Table 4. Findings of the Sulforhodamine B Cytotoxicity Assay against Three Distinct Cancer Cell Lines (Caco-2, HepG-2, and MCF-7) and One Normal Cell Line (Vero Cells)[a]

compound	mean IC$_{50}$ Caco-2 (μM) ± SD	mean IC$_{50}$ HepG-2 (μM) ± SD	mean IC$_{50}$ MCF-7 (μM) ± SD	nean IC$_{50}$ Vero cells (μM)
1	>100	>100	7.68 ± 0.51	>100
2	>100	>100	6.27 ± 0.35	>100
3a	>100	>100	10.23 ± 1.00	>100
3b	>100	58.37 ± 4.19	8.57 ± 0.46	>100
3c	69.36 ± 6.55	79.10 ± 7.45[b]	10.86 ± 1.55	>100
3d	>100	>100	21.62 ± 2.97[a,b,c,d,#]	>100
3e	>100	59.69 ± 4.58	>100	>100
3f	>100	>100	32.17 ± 2.02[a,b,c,d#,@,&]	>100
4a	80.29 ± 6.62[#]	>100	35.08 ± 1.07[a,b,c,d,#,@]	>100
4b	31.40 ± 0.53[#,?]	27.15 ± 2.23[b,Δ,#]	21.71 ± 2.14[a,b,c,d,#,&,?]	>100
Cs/4b-NSs	16.15 ± 0.66[#,?,e]	26.66 ± 1.18[b,#,Δ]	6.9 ± 0.86[@,&,?,e]	>100
4c	54.50 ± 0.8[#,?,e,f]	79.44 ± 1.77[b,Δ,e,f]	49.61 ± 4.37[a,b,c,d,#,@,&,?,e,f]	>100
4d	36.27 ± 1.72[#,?,f,g]	51.29 ± 1.89[#,e,f,g]	74.76 ± 2.73[a,b,c,d,#,@,&,?,e,f,g]	>100
4e	>100	>100	>100	>100
4f	46.01 ± 1.96[#,?,e,f,γ]	69.52 ± 4.99[e,f,γ]	36.98 ± 0.58[a,b,c,d,#,@,e,f,g,γ]	>100
Rapamycin	27.68 ± 1.63[#,?,f,g,€]	47.55 ± 3.83[#,Δ,e,f,g,€]	5.62 ± 0.24[&,?,e,g,γ,€]	>100
Ribavirin	9.78 ± 0.94[#,?,e,g,γ,€,α]	63.94 ± 3.43[#,e,f,g,γ,α]	10.21 ± 0.15[@,&,?,e,g,γ,€]	>100

[a]Data are represented as the mean ± SD. Statistical analysis was carried out using one-way ANOVA test followed by a Tukey posthoc test (P ranged from <0.05 to <0.0001). The symbols mean a significant difference as compared with (a) compound 1, (b) compound 2, (c) 3a, (d) 3b, (#) 3c, (@) 3d, (&) 3f, (?) 4a, (e) 4b, (f) Cs/4b-NSs, (€) 4f, (g) 4c, (γ) 4d, (Δ) 3e, and (α) Rapamycin.

68.9% increases in the cytotoxicity with IC$_{50}$ values of 16.15, 26.66, and 6.90 μM against Caco-2, HepG-2, and MCF-7 cells, respectively (Figure 7B−D and Table 4).

2.5. eIF4E/p-eIF4E Expression Mechanism Assay. One of the main features of cancer onset and progression is the malfunctioning of the translation machinery, resulting in increased protein synthesis due to eIF4E dysregulation.[56,57] eIF4E was proven to be highly expressed in the most aggressive breast cancers, and it was also found that p-eIF4E was more expressed in the MCF-7 cells than the unphosphorylated protein. The dysregulation of such protein is proven to cause aberrant translation of oncogenes and growth-promoting factors.[58] Thus, the western blot technique was utilized to measure the total protein expression of both eIF4E and p-eIF4E. Since the cytotoxicity results of the majority of the synthesized compounds showed pronounced cell killing against the MCF-7 cells, these cells were chosen to further exploit the tendency of the most active compounds to inhibit the targeted protein (eIF4E). The assay was carried out on MCF-7 cells treated with 3b, 3c, 4b, Cs/4b-NSs, and 4f, compared to Ribavirin as the positive control drug. Results are demonstrated in Table 5 and Figure 8. Notably, the nanoparticle niosomes showed significant enhancement of inhibition by 5.89% of total eIF4E protein compared to the drug 4b itself. In addition, a comparable inhibition of the p-eIF4E protein was noticed with the same treatment groups, where Cs/4b-NSs showed 8% less p-eIF4E compared to the 4b synthesized drug.

The results revealed that the expression of p-eIF4E in the untreated malignant cells was more than that of the unphosphorylated eIF4E protein by around 20.4%. Treatment with Ribavirin caused a 53% decrease in p-eIF4E and a 32.1% decrease in eIF4E protein. Previous studies reported that the activity of the oncogene eIF4E is increased via its phosphorylation at serine amino acid. At the same time, the unphosphorylated moiety is not the main responsible component for its conversion to an oncogene.[20] Treatment with compounds 3c, 4b, Cs/4b-NSs, and 4f showed inhibition in the expression of p-eIF4E by 13, 35.8, 40.7, and 25.6%,

respectively, compared to the untreated control. On the other hand, protein expression of the nonphosphorylated form was increased in the treated groups, where 3b, 3c, 4b, Cs/4b-NSs, and 4f showed 1-fold, 20%, 31%, 6%, and 15% increases, respectively, compared to the MCF-7 cells. These findings align with previous studies that reported that the knock-in mice expressing a nonphosphorylated form of eIF4E are resistant to tumorigenesis.[59] Thus, it is suggested that treatment increases the unphosphorylated moiety of the target protein to hinder the formation of cancer cells and aid in the treatment progression.

3. CONCLUSIONS

We developed 15 novel GMP-based analogs with an N7 benzyl group and different phosphoramidated derivatives. The designed compounds showed in silico-promising pharmacokinetic and pharmacodynamic properties. Compounds were subjected to in vitro cytotoxic studies against Caco2, Hepg2, and MCF-7 cell lines and exhibited promising antiproliferative activity, especially against breast cancer type compared to Ribavirin. In addition, the compounds showed no cytotoxic activity against normal Vero cell lines. Compound 4b was the most active compound against the three cell lines subjected to this investigation, and hence, it was selected to be loaded into chitosan-coated niosome (CS/4b-NSs). The developed CS/4b-NSs showed a remarkable improvement in the cytotoxic activity as compared to free 4b. Moreover, the total protein expression of both eIF4E and p-eIF4E was measured to reveal the mechanism of antitumor activity expressed by the new drugs in MCF-7 cells. Selected compounds 3b, 3c, 4b, 4f, and CS/4b-NSs showed comparable inhibition of p-eIF4E with the best 40.7% inhibition displayed by CS/4b-NSs. Our findings proved that the kinetically enhanced approach of loading compound 4b in niosomal nanovesicles could be a promising approach for targeted cancer therapy.
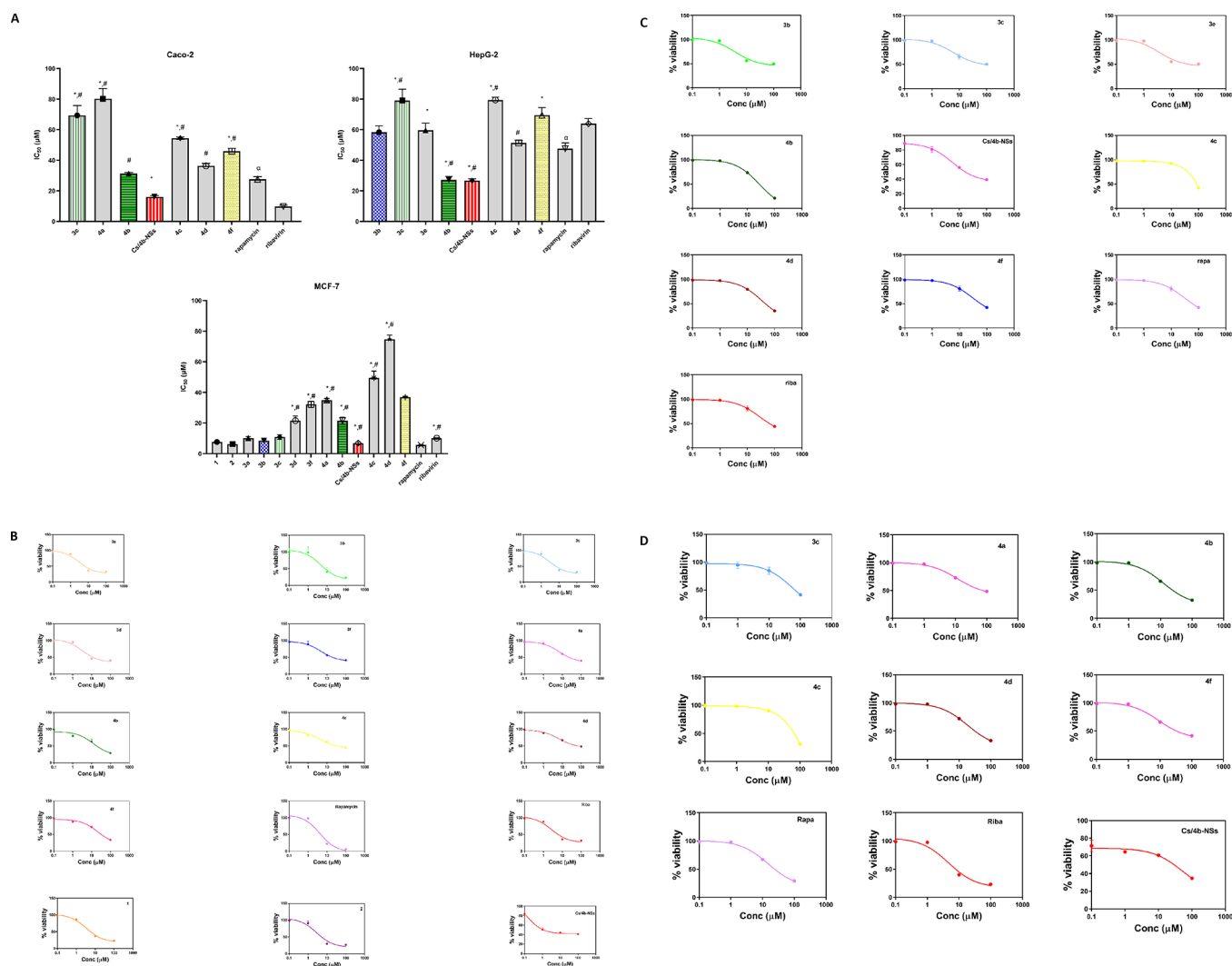
Figure 7. (A) IC_{50} expressed by the novel compounds with evident activity against Caco-2, HepG-2, and MCF-7 cells. Data are represented as the mean $\pm$ SD ($n = 3$). Statistical analysis was carried out using one-way ANOVA test followed by a Tukey posthoc test (P ranged from <0.05 to <0.0001). The symbols mean significant differences compared to (*) rapamycin and (#) Ribavirin. (B) Collective dose−response curves of novel compounds with evident activity against MCF-7 cells. Data are represented as the mean $\pm$ SD ($n = 3$). Compounds with IC_{50} over 100 were not represented within curves. (C) Collective dose−response curves of novel compounds with evident activity against HepG-2 cells. Data are represented as the mean $\pm$ SD ($n = 3$). Compounds with IC_{50} over 100 were not represented within curves. (D) Collective dose−response curves of novel compounds with evident activity against Caco-2 cells. Data are represented as the mean $\pm$ SD ($n = 3$). Compounds with IC_{50} values over 100 were not represented within curves.

4. EXPERIMENTAL SECTION

4.1. Materials and Instrumentation. Melting points (°C) were determined by the open capillary tube method using a Bio Cote SMP 10 apparatus, and they are uncorrected. Microanalyses were performed using a FLASH 2000 CHNS/O analyzer, Thermo Scientific at the Regional Center for Mycology and Biotechnology (RCMB), Al-Azhar University, Nasr City, Cairo. All new compounds were analyzed for C, H, and N and agreed with the proposed structures within ±0.4% of the theoretical values. The IR spectra were recorded on a Shimadzu FT-IR 8400S infrared spectrophotometer affinity A1 and expressed as wavenumber (cm^{-1}) using potassium bromide disks at the microanalytical unit, Faculty of Pharmacy, Cairo University. The FTIR spectral data of niosomes were obtained using an FTIR-8400s instrument (Shimadzu, Kyoto, Japan). ^{1}H and ^{13}C NMR spectra were carried out at the NMR unit, Faculty of Pharmacy Mansoura University, using a Bruker High-performance Digital FT-NMR spectrometer Avance III

400 MHz for ^{1}H NMR and 100 MHz for ^{13}C NMR. Chemical shifts are expressed in δ ppm with reference to TMS. The mass spectra were carried out on the Direct Inlet part to the mass analyzer in Thermo Scientific GCMS model ISQ at the Regional Center for Mycology and Biotechnology (RCMB), Al-Azhar University, Nasr City, Cairo. Thin-layer chromatography was performed on precoated (0.25 mm) silica gel GF$_{254}$ plates (E. Merck, Germany), and compounds were detected with a 254 nm UV lamp. Silica gel (60−230 mesh) was employed for routine column chromatography separations using CHCl$_3$/MeOH/H$_2$O (5:2:0.25, containing 0.5% NH$_4$OH).

4.2. Synthesis of Target Compounds. *4.2.1. General Procedure for the Synthesis of Sodium(5-(2-benzamido-6-oxo-1,6-dihydro-9H-purin-9-yl)-3,4-dihydroxyterahydrofuran-2-yl) Methyl Phosphate (1).* In a flask, 0.25 g of GMP was dissolved in 5 mL of absolute ethanol, and benzoyl chloride was added (1.5 mL) in a ratio of 1.5:1 mol. Reflux started at

Table 5. Total Protein Expression of Both eIF4E/*p*-eIF4E upon MCF-7 Cells' Treatment by the Synthesized Novel Compounds[a]

lane	group	**protein	mean protein (ng/mL)	protein ratio normalized to reference protein	change in fold
1	MCF7 cells	β-actin	4.352	82.6	
		eIF4E	3.285	62.8	1
		p-eIF4E	4.051	75.6	1
2	Ribavirin	β-actin	3.118	72.2	
		eIF4E	2.520	42.6*	0.68
		p-eIF4E	2.190	35.5*	0.47
3	compound 3c	β-actin	5.825	112.2	
		eIF4E	4.118	75.6*	1.20
		p-eIF4E	3.812	65.8*,#	0.87
4	compound 4f	β-actin	5.172	125.2	
		eIF4E	4.226	72.5*,#	1.15
		p-eIF4E	3.204	56.2*,#,@	0.74
5	compound Cs/4b-NSs	β-actin	4.200	132.6	
		eIF4E	3.560	66.5#,@	1.06
		p-eIF4E	3.860	44.8*,#,@,&	0.59
6	compound 3b	β-actin	5.290	155.6	
		eIF4E	3.221	135.5*,#,@,&,α	2.16
		p-eIF4E	3.072	78.2#,@,&,α	1.03
7	compound 4b	β-actin	3.180	110.2	
		eIF4E	2.150	82.5*,#,@,&,α,μ	1.31
		p-eIF4E	2.760	48.5*,#,@,μ	0.64

[a]Data are presented as the mean ± SD ($n = 3$). Statistical analysis was carried out using one-way ANOVA test followed by a Tukey posthoc test ($P \ll 0.0001$). The symbols mean a significant difference as compared with (*) MCF-7 control, (#) Ribavirin, (@) 3c, (&) 4f, (α) Cs/4b-NSs, and (μ) 3b

100 °C for 24 h after adding 1 μL of pyridine dropwise. The yielded product was poured onto ice, left for 24 h, and filtered. The filtrate was further evaporated under a vacuum to yield a pure compound (1)[29]

The compound was separated as white crystals (89%): mp 220−222 °C; ^{1}H NMR (DMSO, 400 MHz): δ 1.06 (s, 1H, NH (D$_2$O-exchangeable)), 1.23 (s, 1H, NH (D$_2$O-exchangeable)), 1.913 (s, 1H, OH (D$_2$O-exchangeable)), 2.08 (s, 1H, OH, D$_2$O-exchangeable), 3.42−3.47 (m, 7H, tetrahydrofuran, and CH$_2$), 3.51 (s,1H, imidazole H), 7.47−7.51 (t, J = 7.6 Hz, 2H, ArH), 7.59−7.63 (t, J = 7.2 Hz, 1H, ArH), 7.93−7.95 (d, J = 7.2 Hz, 2H, ArH); ^{13}C NMR: δ 65.7, 70.7, 74.1, 83.6, 83.7, 87.7, 119.1, 126.0, 129.0, 131.1, 133.3, 140.8, 149.5, 150.1, 154.1, 167.8. IR (KBr): 3303, 1634 cm^{-1}; [M]+ calcd. for C$_{17}$H$_{16}$N$_5$Na$_2$O$_9$P, 511.29; found, 511.07; analysis (calcd., found for C$_{17}$H$_{16}$N$_5$Na$_2$O$_9$P): C (39.96, 40.18), H (3.15, 3.31), N (13.70, 13.97).

4.2.2. General Procedure for the Synthesis of Sodium(6-(2-benzamido-6-oxo-1,6-dihydro-9H-purin-9-yl)-2,2-dimethyltetrahydrofuro[3,4-d][1,3]dioxol-4-yl)-methylphosphate (2). Compound 2 was then prepared by reacting previously prepared intermediate 1 (0.06 g, 0.0001 mol) dissolved in methylene chloride (5 mL) with 2,2-dimethoxypropane (0.014 mol, 1.5 mL) in the presence of *p*-toluenesulfonic acid monohydrate (97%, 0.1 g) as a catalyst. The reaction was applied at 150 °C and under reflux for 24 h. The product was also poured onto ice, filtered off directly with several runs of methylene chloride, and then dried off.[30]

The title compound was separated as white crystals (93%); mp 180−182 °C. ^{1}H NMR (DMSO, 400 MHz): δ 3.93−3.98 (q, J = 6.0 Hz, 1H, CH), 4.04 (s, 6H, CH$_3$), 4.11−4.12 (d, J = 4.4 Hz, 1H, CH), 4.43−4.46 (t, J = 5.6 Hz, 2H, CH), 5.72−5.73 (d, J = 6.0 Hz, 2H, CH$_2$), 6.83 (s, 1H, imidazole H), 7.74−7.78 (t, J = 6.4 Hz, 2H, ArH), 7.93−7.95 (d, J = 8.8 Hz, 2H, ArH), 8.21−8.25 (t, J = 8.4 Hz, 1H, ArH), 8.77 (s, 2H, NH, D$_2$O-exchangeable); ^{13}C NMR: δ 21.3, 56.2, 74.5, 78.1, 82.5, 87.1, 125.6, 128.2, 129.3, 130.9, 132.1, 137.6, 139.9, 140.6, 149.8, 162.5. [M]+ calcd. for C$_{20}$H$_{20}$N$_5$Na$_2$O$_9$P, 511.29; found, 544.92; analysis (calcd., found for C$_{20}$H$_{20}$N$_5$Na$_2$O$_9$P): C (39.96, 40.18), H (3.15, 3.31), N (13.70, 13.97).

4.2.3. General Procedure for the Synthesis of Compounds 3a−3f. Phosphoramidation reaction was carried out by reacting 0.7 g (0.0013 mol) of yielded compound 2 with 0.002 mol of the desired amine in a one-pot reaction dissolved in absolute ethanol (6 mL) and was allowed to react using 0.05 g of DCC and reflux for 48 h. The product mixture was concentrated in vacuo, and the residue was chromatographed on silica gel, eluting with CHCl$_3$/MeOH/H$_2$O (5:2:0.25, containing 0.5% NH$_4$OH).[19]

4.2.3.1. Sodium(6-(2-benzamido-6-oxo-1,6-dihydro-9H-purin-9-yl)-2,2-dimethyltetrahydro furo[3,4-d][1,3]dioxol-4-yl)methyl(2-caboxyethyl)phosphoramide (3a). The title compound was separated as light brown crystals (72%); mp 144−147 °C. ^{1}H NMR (CDCl$_3$, 400 MHz): δ 1.09−1.15 (m, 2H, CH$_2$), 1.21−1.27 (m, 6H, CH$_3$), 1.54−1.62 (m, 2H, CH$_2$), 1.96−2.08 (m, 1H, CH), 3.48−3.50 (m, 2H, CH), 3.68−3.75 (s, 2H, CH$_2$), 4.07−4.13 (d, J = 8.0 Hz, 1H, CH), 7.38−7.42 (m, 2H, ArH and imidazole H), 7.45−7.46 (m, 2H, ArH), 7.53−7.55 (d, J = 6.8 Hz, 2H, ArH), 7.77−7.86 (m, 4H, 3NH, OH (D$_2$O-exchangeable)); ^{13}C NMR: δ 14.5, 21.23, 25.8, 30.7, 31.9, 32.9, 33.7, 35.1, 36.2, 47.9, 52.2, 60.9, 125.9, 129.6, 138.5, 145.5, 159.0, 169.0, 170.8, 171.3, 173.9. IR (KBr): 3402, 3201, 1685 cm^{-1}; [M]+ calcd. for C$_{23}$H$_{26}$N$_6$NaO$_{10}$P$^+$, 600.46; found, 600.69; analysis (calcd., found for C$_{23}$H$_{26}$N$_6$NaO$_{10}$P$^+$): C (46.01, 46.25), H (4.36, 4.58), N (14.00, 14.17).

4.2.3.2. Sodium(6-(2-benzamido-6-oxo-1,6-dihydro-9H-purin-9-yl)-2,2-dimethyltetrahydro furo[3,4-d][1,3]dioxol-4-yl)methyl(2-(2,4-dinitrophenyl)hydrazinyl)phosphonate (3b). The title compound was separated as brown crystals (65%); mp 133−135 °C. ^{1}H NMR (DMSO, 400 MHz): δ 3.08−3.13 (m, 1H, CH), 3.76 (s, 1H, CH), 4.13−4.19 (t, J = 11.2 Hz, 2H, CH), 5.04 (s, 2H, CH$_2$), 7.35−7.38 (m, 2H, ArH and imidazole H), 7.44−7.48 (m, 3H, ArH), 7.50 (s, 1H, ArH), 7.67−7.69 (d, J = 9.6 Hz, 1H, ArH), 7.82−7.84 (d, J = 7.6 Hz, 2H, ArH), 7.94−7.96 (d, 1H, NH (D$_2$O-exchangeable)), 8.00−8.02 (d, 1H, NH (D$_2$O-exchangeable)), 8.16−8.18 (d, 1H, NH (D$_2$O-exchangeable)), 8.25−8.28 (d, 1H, NH (D$_2$O-exchangeable)), 8.82 (s, 1H, NH (D$_2$O-exchangeable)); ^{13}C NMR: δ 14.9, 21.2, 24.6, 24.9, 26.0, 30.8, 31.7, 33.8, 47.9, 49.5, 116.9, 119.0, 124.1, 125.9, 127.4, 128.5, 130.3, 132.1, 135.6, 136.9, 138.2, 141.6, 146.0, 152.1, 156.8. IR (KBr): 3485, 3271, 3186, 1875 cm^{-1}; [M]+ calcd. for C$_{26}$H$_{25}$N$_9$NaO$_{12}$P$^+$, 709.49; found, 708.78; analysis (calcd., found for C$_{26}$H$_{25}$N$_9$NaO$_{12}$P$^+$); C (44.01, 44.20), H (3.55, 3.38), N (17.77, 16.98).

4.2.3.3. Sodium(6-(2-benzamido-6-oxo-1,6-dihydro-9H-purin-9-yl)-2,2-dimethyltetrahydro furo[3,4-d][1,3]dioxol-4-yl)methyl(4-(2-morpholinoethyl)phenyl)phosphoramidate (3c). The title compound was separated as a buff powder (60%); mp 184−187 °C. ^{1}H NMR (CDCl$_3$, 400 MHz): δ 1.81−1.33 (m, 6H, CH$_3$), 1.53 (s, 4H, CH$_2$), 1.57−1.59 (m, 3H, CH), 1.73−1.78 (m, 4H, CH$_2$), 1.82−1.85 (m, 4H, CH$_2$),
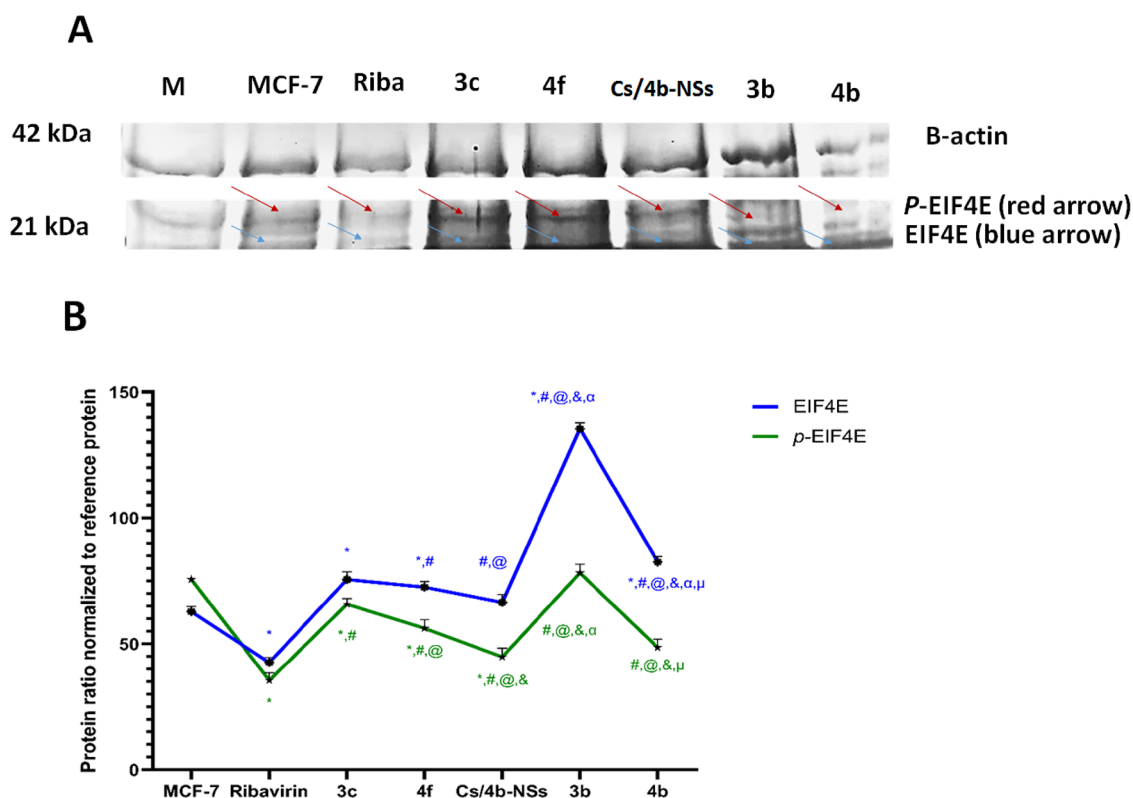
Figure 8. Total protein expression of both eIF4E and p-eIF4E on treated MCF-7 cells. (A) Western blot depicting the protein expression levels of eIF4E and p-eIF4E. (B) Relative protein expression levels normalized to beta-actin control. Data are presented as the mean ± SD ($n = 3$). Statistical analysis was carried out using one-way ANOVA test followed by Tukey posthoc test ($P < 0.0001$). The symbols mean a significant difference as compared with (*) MCF-7 control, (#) Ribavirin, (@) **3c**, (&) **4f**, (α) Cs/**4b**-NSs, and (μ) **3b**.

1.94 (s, 1H, NH (D$_2$O-exchangeable)), 2.02−2.04 (d, J = 11.6 Hz, 1H, CH), 3.46−3.48 (m, 1H, CH), 3.99−4.16 (m, 1H, CH), 7.19−7.21 (d, J = 8.0 Hz, 1H, ArH), 7.38−7.41 (m, 2H, ArH and imidazole H), 7.45−7.49 (m, 2H, ArH), 7.55−7.62 (m, 2H, ArH), 7.78−7.80 (d, J = 8 Hz, 1H, ArH), 8.09−8.11 (d, J = 7.2 Hz, 2H, ArH); ^{13}C NMR: δ 14.9, 15.5, 24.9, 25.9, 28.9, 34.0, 48.0, 51.4, 56.7, 63.7, 112.8, 119.9, 122.5, 123.9, 125.9, 128.9, 131.9, 132.9, 135.5, 136.2. 149.6, 151.3, 154.1, 157.3, 160.3. IR (KBr): 3303, 1634 cm^{-1}; [M]+ calcd. for C$_{32}$H$_{37}$N$_7$NaO$_9$P$^+$, 717.65; found, 717.23; analysis (calcd., found for C$_{32}$H$_{37}$N$_7$NaO$_9$P$^+$): C (53.56, 53.38), H (5.20, 4.98), N (13.66, 13.47).

4.2.3.4. Sodium(6-(2-benzamido-6-oxo-1,6-dihydro-9H-purine-9-yl)-2,2-dimethyltetrahydro furo[3,4-d][1,3]dioxol-4-yl)methyl(4-(4-phenylpiperazine-1-yl)phenyl)-phosphoramidate (3d). The title compound was separated as a white powder (67%); mp 185−188 °C. ^{1}H NMR (CDCl$_3$, 400 MHz): δ 1.35 (s, 1H, NH (D$_2$O-exchangeable)), 1.54−1.60 (m, 6H, CH$_3$), 1.71−1.82 (m, 4H, CH), 3.44−3.47 (t, J = 4.4 Hz, 4H, CH$_2$), 3.69−3.71 (t, J = 4.8 Hz, 4H, CH$_2$), 4.10−4.13 (d, J = 12 Hz, 2H, CH$_2$), 6.88−6.91 (d, J = 9.6 Hz, 1H, ArH), 7.05 (s, 1H, NH (D$_2$O-exchangeable)), 7.19−7.21 (d, J = 8 Hz, 1H, ArH), 7.34 (s, 1H, NH (D$_2$O-exchangeable)), 7.38 (s, 1H, NH (D$_2$O-exchangeable)), 7.40−7.42 d, J = 7.6 Hz, 2H, ArH), 7.46−7.49 (m, 3H, 2ArH and imidazole H), 7.55−7.62 (m, 3H, ArH), 7.79−7.81 (d, J = 8.0 Hz, 1H, ArH), 8.10−8.12 (d, J = 7.2 Hz, 2H, ArH), 8.14−8.16 (d, J = 9.0 Hz, 2H,ArH); ^{13}C NMR: δ 25.9, 29.6, 30.5, 38.5, 47.9, 51.0, 52.7, 53.7, 68.4, 118.0, 121.5, 125.6, 130.7, 131.0, 132.3, 133.3, 134.3, 142.3, 143.0, 147.3, 150.3, 154.7, 159.7, 161.9. IR (KBr): 3369, 1698 cm^{-1}; [M]+ calcd. for C$_{36}$H$_{38}$N$_8$NaO$_8$P$^+$,

764.71; found, 764.35; analysis (calcd., found for C$_{36}$H$_{38}$N$_8$NaO$_8$P$^+$): C (56.54, 56.32), H (5.01, 4.89), and N (14.65, 14.44).

4.2.3.5. Sodium(6-(2-benzamido-6-oxo-1,6-dihydro-9H-purin-9-yl)-2,2-dimethyltetrahydro furo[3,4-d][1,3]dioxol-4-yl)methyl(4-(p-tolyl)thiazole-2-yl)phosphoramidate (3e). The title compound was separated as a white powder (66%); mp 192−194 °C. ^{1}H NMR (CDCl$_3$, 400 MHz): δ 2.37 (s, 3H, CH$_3$), 2.40 (s, 6H, CH$_3$), 3.48−3.50 (m, 4H, CH), 4.07 (s, 1H, NH (D$_2$O-exchangeable)), 4.09−4.11 (t, J = 6.4 Hz, 2H, CH$_2$), 4.13 (s, 1H, NH (D$_2$O-exchangeable)), 7.41−7.73 (d, J = 6.4 Hz, 2H, ArH), 7.45−7.49 (m, 2H, ArH and imidazole H), 7.54−7.56 (m, 3H, 2ArH and thiazole-H), 7.60−7.64 (t, J = 8.8 Hz, 3H, ArH), 7.71−7.73 (d, J = 8 Hz, 1H, ArH), 7.81−7.83 (m, 1H, NH (D$_2$O-exchangeable)); ^{13}C NMR: δ 21.2, 24.9, 25.8, 33.8, 43.2, 47.9, 68.4, 101.5, 125.9, 128.6, 129.7, 138.5, 145.4, 145.5, 169.6. IR (KBr): 3352, 3285, 1634 cm^{-1}; [M]+ calcd. for C$_{30}$H$_{29}$N$_7$NaO$_8$P$^+$S, 703.63/701.63; found, 703.14/701.32; analysis (calcd., found for C$_{30}$H$_{29}$N$_7$NaO$_8$P$^+$S): C (51.36, 51.53), H (4.17, 4.31), and N (13.97, 14.20).

4.2.3.6. Sodium(6-(2-benzamido-6-oxo-1,6-dihydro-9H-purin-9-yl)-2,2-dimethyltetrahydro furo[3,4-d][1,3]dioxol-4-yl)methyl Thiazol-2-ylphosphoramidate (3f). The title compound was separated as a white powder (63%); mp 186−188 °C. ^{1}H NMR (CDCl$_3$, 400 MHz): δ 1.20−1.26 (m, 3H, CH$_3$), 1.53−1.59 (m, 5H, CH$_2$,CH$_3$), 1.81−1.84 (m, 3H, CH), 2.02−2.05 (d, J = 12.4 Hz, 1H, CH), 3.48 (s, 1H, NH (D$_2$O-exchangeable)), 4.08−4.14 (m, 1H, NH (D$_2$O-exchangeable)), 6.95−6.96 (d, J = 3.6 Hz, 1H, thiazole H), 7.10−7.11 (d, J = 3.6 Hz, 1H, thiazole H), 7.39−7.41 (m, 1H,

ArH), 7.52 (s, 1H, imidazole H), 7.54–7.55 (m, 1H, ArH), 7.61–7.64 (t, J = 8 Hz, 1H, ArH), 7.77–7.79 (m, 1H, NH (D$_2$O-exchangeable)), 8.04–8.06 (d, J = 8.0 Hz, 1H, ArH); ^{13}C NMR: δ 21.2, 24.8, 25.7, 33.7, 35.9, 38.1, 39.2, 43.12, 47.9, 58.5, 63.6, 107.4, 122.1, 125.9, 129.7, 131.3, 133.3, 135.9, 145.1, 168.4, 169.7, 171.9. IR (KBr): 3271, 3183, 1745 cm^{-1}; [M]+ calcd. for C$_{23}$H$_{23}$N$_7$NaO$_8$P$^+$S, 613.50/611.50; found, 613.10/611.22; analysis (calcd., found C$_{23}$H$_{23}$N$_7$NaO$_8$P$^+$S) C (45.18, 45.39), H (3.79, 4.02), N (16.03, 16.27).

4.2.4. General Procedure for the Synthesis of Compounds 4a–4f. In a flask containing 5 mL of methylene chloride, 0.2 mmol of the previously prepared amines was dissolved. A total of 0.5 mL of benzyl bromide was then added, and the reaction mixture was subjected to gentle heating for 1h followed by stirring at room temperature for 48 h. The yielded product was filtered off, washed with methylene chloride, and dried through vacuum.[27]

4.2.4.1. (6-(2-Benzamido-7-benzyl-6-oxo-1,6-dihydro-9H-purin-7-ium-9-yl)-2,2-dimethyl tetrahydrofuro[3,4-d][1,3]-dioxol-4-yl)methyl(2-carboxyethyl)phosphoramidate Sodium Salt (4a). The title compound was separated as a pink powder (86%); mp 107–109 °C. ^{1}H NMR (CDCl$_3$, 400 MHz): δ 1.54 (s, 1H, CH), 1.59–1.62 (d, J = 12 Hz, 2H, CH), 1.72 (s, 1H, NH (D$_2$O-exchangeable)), 1.79–1.84 (m, 6H, CH$_3$), 1.92–1.95 (m, 2H, CH), 2.04–2.07 (d, J = 11.6 Hz, 2H, CH$_2$), 2.68 (s, 1H, NH (D$_2$O-exchangeable)), 2.75 (s, 1H, NH (D$_2$O-exchangeable)), 3.47–3.51 (m, 2H, CH), 3.73 (s, 2H, CH$_2$), 4.06–4.12 (t, J = 12.0 Hz, 1H, CH), 6.18 (s, 1H, imidazole H), 7.38–7.42 (m, 3H, ArH), 7.44–7.48 (m, 3H, ArH), 7.53–7.55 (m, 3H, ArH), 7.77–7.80 (t, J = 7.2 Hz, 1H, ArH), 7.84–7.86 (m, 1H, OH (D$_2$O-exchangeable)); ^{13}C NMR: δ 21.2, 23.4, 23.9, 25.4, 31.6, 35.2, 38.6, 51.0, 53.3, 114.8, 117.8, 119.2, 125.7, 129.0, 130.9, 136.5, 139.7, 143.4, 168.7, 172.4. IR (KBr): 3502, 3189, 1764 cm^{-1}; [M]+ calcd. for C$_{30}$H$_{33}$BrN$_6$NaO$_{10}$P$^+$, 773.86/771.49; found, 778.16/776.29; analysis (calcd., found for C$_{30}$H$_{33}$BrN$_6$NaO$_{10}$P$^+$) C (46.71, 46.41), H (4.31, 4.48), N (10.89, 10.72).

4.2.4.2. (6-(2-Benzamido-7-benzyl-6-oxo-1,6-dihydro-9H-purin-7-ium-9-yl)-2,2-dimethyl tetrahydrofuro[3,4-d][1,3]-dioxol-4-yl)methyl(2-(2,4-dinitrophenyl)hydrazinyl)-phosphate Sodium Salt (4b). The title compound was separated as an orange powder (89%); mp 110–112 °C. ^{1}H NMR (CDCl$_3$, 400 MHz): δ 1.76–1.82 (m, 6H, CH$_3$), 2.02–2.05 (m, 3H, CH), 3.50 (s, 1H, CH), 3.85–3.97 (m, 2H, CH$_2$), 4.13–4.16 (m, 2H, CH$_2$), 7.28–7.32 (m, 3H, ArH), 7.38 (s, 1H, imidazole H), 7.40–7.44 (m, 3H, ArH), 7.48–7.49 (d, J = 5.6 Hz, 2H, ArH), 7.53–7.55 (d, J = 7.6 Hz, 2H, ArH), 7.73–7.75 (d, J = 6.8 Hz, 2H, ArH), 8.03–8.05 (m, 1H, ArH), 8.23–8.25 (d, 1H, NH (D$_2$O-exchangeable)), 8.36–8.39 (d, 1H, NH (D$_2$O-exchangeable)), 8.9 (s, 1H, NH (D$_2$O-exchangeable)), 9.07–9.16 (t, 1H, NH (D$_2$O-exchangeable)); ^{13}C NMR: δ 21.2, 23.0, 24.1, 24.8, 24.9, 25.7, 30.6, 32.7, 33.6, 35.2, 48.1, 48.8, 49.8.63.1, 120.2, 123.8, 125.9, 127.8, 128.5, 128.7, 129.7, 135.5, 138.7, 145.0, 157.3, 166.0. IR (KBr): 3485, 3271, 3186, 1875 cm^{-1}; [M]+ calcd. for C$_{33}$H$_{32}$BrN$_9$NaO$_{12}$P$^+$, 883.63/880.24; found, 883.19/880.93; analysis (calcd., found for C$_{33}$H$_{32}$BrN$_9$NaO$_{12}$P$^+$) C (45.01, 45.21), H (3.66, 3.87), N (14.32, 14.57).

4.2.4.3. (6-(2-Benzamido-7-benzyl-6-oxo-1,6-dihydro-9H-purin-7-ium-9-yl)-2,2-dimethyl tetrahydrofuro[3,4-d][1,3]-dioxol-4-yl)methyl(4-(2-morpholinoethyl)phenyl)-phosphoramidate Sodium Salt (4c). The title compound was separated as a brown powder (88%); mp 101–103 °C. ^{1}H

NMR (DMSO, 400 MHz): δ 1.59–1.62 (m, 4H, CH$_2$), 1.72 (s, 6H, CH$_3$), 1.78–1.82 (m, 4H, CH$_2$), 1.88–1.89 (m, 1H, CH), 2.96–3.03 (q, J = 8.4 Hz, 1H, CH), 3.09–3.15 (m, 2H, CH), 3.66–3.70 (m, 2H, CH$_2$), 3.82 (s, 2H, CH$_2$), 4.00–4.03 (d, J = 12.4 Hz, 2H, CH$_2$), 4.12–4.18 (t, J = 11.6 Hz, 2H, CH$_2$), 6.80–6.82 (d, J = 7.6 Hz, 1H, ArH), 7.11–7.13 (d, J = 7.6 Hz, 3H, ArH and imidazole H), 7.25–7.27 (d, J = 8.4 Hz, 1H, ArH), 7.36–7.38 (d, J = 7.2 Hz, 2H, ArH), 7.42(s, 1H, NH (D$_2$O-exchangeable)), 7.44–7.45 (d, J = 4.0 Hz, 1H, ArH), 7.46–7.48 (m, 3H, ArH), 7.50–7.53 (m, 4H, ArH), 7.54 (s, 1H, NH (D$_2$O-exchangeable)), 7.62 (s, 1H, NH (D$_2$O-exchangeable)); ^{13}C NMR: δ 21.5, 24.8, 25.7, 27.6, 30.6, 32.8, 33.7, 46.3, 48.0, 51.5, 51.8, 53.3, 56.9, 58.1, 63.6, 108.1, 120.8, 125.9, 128.5, 128.7, 129.9, 132.5, 134.5, 138.9, 142.2, 145.6, 151.2, 155.6, 157.0, 167.3, 167.7. IR (KBr): 3251, 1843 cm^{-1}; [M]+ calcd. for C$_{39}$H$_{44}$BrN$_7$NaO$_9$P$^+$, 890.12/888.69; found, 890.45/888.38; analysis (calcd., found for C$_{39}$H$_{44}$BrN$_7$NaO$_9$P$^+$) C (52.71, 52.85), H (4.99, 5.51), N (11.03, 11.23).

4.2.4.4. (6-(2-Benzamido-7-benzyl-6-oxo-1,6-dihydro-9H-purin-7-ium-9-yl)-2,2-dimethyl tetrahydrofuro[3,4-d][1,3]-dioxol-4-yl)methyl(4-(4-phenylpiperazin-1-yl)phenyl)-phosphoramidate Sodium Salt (4d). The title compound was separated as a yellow powder (82%); mp 126–128 °C. ^{1}H NMR (DMSO, 400 MHz): δ 1.60 (s, 2H,CH$_2$), 1.72–1.74 (m, 6H, CH$_3$), 1.78–1.82 (d, J = 12 Hz, 2H, CH$_2$), 1.86 (s, 2H, CH), 2.28 (s, 2H, CH$_2$), 3.09–3.12 (q, J = 6.0 Hz, 1H, CH), 3.13 (s, 1H, CH), 3.61–3.62 (d, J = 5.2 Hz, 4H, CH$_2$), 3.80–3.81 (s, 2H, CH$_2$), 4.15–4.21 (m, 2H, CH$_2$), 6.80–6.85 (m, 1H, ArH), 6.98–7.00 (d, J = 8 Hz, 1H, ArH), 7.07–7.12 (m, 3H, ArH), 7.23–7.26 (t, J = 7.2 Hz, 1H, ArH), 7.32 (s, 1H, NH (D$_2$O-exchangeable)), 7.36–7.38 d, J = 7.6 Hz, 1H, ArH), 7.41 (s, 1H, NH (D$_2$O-exchangeable)), 7.43–7.46 (m, 3H, 2ArH and imidazole H), 7.48–7.52 (t, J = 7.6 Hz, 4H, ArH), 7.60–7.64 (t, J = 7.2 Hz, 2H, ArH), 7.82–7.84 (d, 1H, NH (D$_2$O-exchangeable)), 7.93–7.95 (d, J = 7.6 Hz, 3H, ArH), 8.07–8.09 (d, J = 9.2 Hz, 1H,ArH); ^{13}C NMR: δ 21.2, 24.8, 27.8, 29.9, 31.5, 33.4, 38.9, 43.2, 45.6, 47.4, 48.3, 51.9, 55.9, 60.0, 62.9, 63.5, 109.1, 113.6, 121.8, 125.8, 127.9, 132.5, 137.3, 139.2, 141.9, 144.3, 147.3, 155.3, 161.8, 166.2, 167.2, 167.9. IR (KBr): 3267, 1835 cm^{-1}; [M]+ calcd. for C$_{43}$H$_{45}$BrN$_8$NaO$_8$P$^+$, 937.65/935.84; found, 936.91/934.80; analysis (calcd., found for C$_{43}$H$_{45}$BrN$_8$NaO$_8$P$^+$) C (55.19, 55.25), H (4.85, 4.71), N (11.98, 12.17).

4.2.4.5. (6-(2-Benzamido-7-benzyl-6-oxo-1,6-dihydro-9H-purin-7-ium-9-yl)-2,2-dimethyl tetrahydrofuro[3,4-d][1,3]-dioxol-4-yl)methyl(4-(p-tolyl)thiazol-2-yl)phosphoramidate Sodium Salt (4e). The title compound was separated as a grayish brown powder (92%); mp 157–159 °C. ^{1}H NMR (DMSO, 400 MHz): δ 1.59–1.68 (m, 2H,CH), 1.71–1.75 (m, 6H, CH$_3$), 1.79 (s, 3H, CH$_3$), 2.29 (s,1H, CH) 2.33 (s, 2H, CH$_2$), 3.07–3.12 (m, 2H, CH$_2$), 4.13–4.19 (m, 1H, CH), 7.11–7.13 (d, J = 8.0 Hz, 2H, ArH), 7.24–7.26 (d, J = 8.0 Hz, 2H, ArH), 7.31 (s, 1H, NH (D$_2$O-exchangeable)), 7.34 (s, 1H, NH (D$_2$O-exchangeable)), 7.36–7.38 (d, J = 7.6 Hz, 2H, ArH), 7.41 (s, 1H, ArH), 7.43–7.45 (m, 2H, ArH and imidazole H), 7.47–7.49 (m, 3H, 2 ArH and thiazole H), 7.54–7.58 (m, 1H, ArH), 7.60–7.65 (m, 1H, ArH), 7.83–7.85 (d, J = 7.2 Hz, 2H, ArH), 7.94–7.96 (d, 1H, NH (D$_2$O-exchangeable)), 8.12–8.14 (d, J = 7.2 Hz, 1H, ArH); ^{13}C NMR: δ 21.3, 24.5, 24.8, 30.7, 31.6, 33.6, 59.06 66.07, 102.8, 108.1, 109.2, 125.9, 126.1, 127.3, 128.5, 128.7, 129.5, 130.1, 141.9, 144.6, 151.6, 154.3, 157.3, 168.7, 170.7. IR (KBr): 3486,

3321, 1754 cm^{-1}; [M]+ calcd. for C$_{37}$H$_{36}$BrN$_7$NaO$_8$PS$^+$, 874.92/872.66; found, 874.45/872.34; analysis (calcd., found for C$_{37}$H$_{36}$BrN$_7$NaO$_8$PS$^+$) C (50.9350.82), H (3.66, 4.24), N (11.24, 11.31).

4.2.4.6. (6-(2-Benzamido-7-benzyl-6-oxo-1,6-dihydro-9H-purin-7-ium-9-yl)-2,2-dimethyl tetrahydrofuro[3,4-d][1,3]-dioxol-4-yl)methylthiazol-2-yl Phosphoramidate Sodium Salt (4f). The title compound was separated as dark brown crystals (89%); mp 140−143 °C. ^{1}H NMR (DMSO, 400 MHz): δ 1.22−1.30 (m, 6H, CH$_3$), 1.59−1.63 (m, 2H, CH), 1.71−1.78 (m, 2H, CH$_2$), 1.81−1.84 (m, 3H, CH), 2.28 (s, 2H, CH$_2$) 3.08−3.12 (m, 1H, CH), 4.16 (s, 1H, NH (D$_2$O-exchangeable)), 5.30 (s, 1H, CH), 7.06−7.08 (m, 1H, NH (D$_2$O-exchangeable)), 7.09−7.14 (m, 2H, ArH), 7.27−7.28 (d, J = 3.6 Hz, 1H, ArH), 7.30−7.32 (d, J = 8 Hz, 1H, ArH), 7.36−7.38 (d, J = 7.2 Hz, 1H, ArH), 7.40−7.41 (d, J = 7.6 Hz, 1H, thiazole H), 7.45−7.47 (m, 2H, ArH and thiazole H), 7.49−7.51 (m, 1H, ArH), 7.54 (s, 1H, imidazole H), 7.55−7.56 (m, 1H, ArH), 7.61−7.65 (t, J = 7.6 Hz, 1H, ArH), 7.83−7.85 (m, 1H, NH (D$_2$O-exchangeable)), 8.08−8.10 (d, J = 7.6 Hz, 1H, ArH); ^{13}C NMR: δ 21.222.9, 24.6, 25.6, 29.9, 33.6, 52.0, 54.7, 57.7, 63.4, 108.9, 114.2, 116.9, 121.2, 125.8, 126.4, 128.8, 130.9, 133.9, 139.2, 144.3, 164.9, 168.4, 170.2. IR (KBr): 3332, 3185, 1754 cm^{-1}; [M]+ calcd. for C$_{30}$H$_{30}$BrN$_7$NaO$_8$PS$^+$, 784.12/782.54; found, 784.52/782.26; analysis (calcd., found for C$_{30}$H$_{30}$BrN$_7$NaO$_8$PS$^+$) C (46.05, 46.21), H (3.86, 3.75), N (12.53, 12.33).

4.3. Computational Studies. *4.3.1. In Silico Docking.* The crystal structure of human eIF4E-4EBP1 peptide complex was downloaded from PDB with code 3U7X,[31] the protein was cleaned, and hydrogen atoms were added.

Simulation with CHARMM charge and MMFF partial charge force fields were applied, and a heavy atom was created. The protein was minimized, and its binding site was defined as downloaded from PDB.

The new synthesized molecules were drawn using ChemDraw V.14 and saved as a mole extension for further view on Discovery Studio Software. Also, reference drug structures were downloaded from PUBCHEM and saved as.Sd. The compounds were simulated with similar force fields to the protein and then prepared as ligands.

Docking procedures were run adopting the C-Docker protocol within Discovery Studio 4.0 using the same force fields applied previously. Results of interaction energies were sorted and recorded together with the binding modes of compounds and viewed via both 3D and 2D view modes.

4.3.2. Standard Dynamic Simulations. The dynamic simulation studies were performed by using Discovery Studio V. 4.0 and applied to free protein and m7G, Ribavirin, and **4b** docked against eIF4E. Standard Dynamic Cascades was applied where the first minimization algorithm was set to the steepest descent with maximum steps of 2000 and RMS gradient of 1.0. The second minimization algorithm was set to the conjugate gradient with maximum steps of 1000. The initial temperature was set to 50, and the target temperature was 300 with a maximum velocity of 2000. On the other hand, the equilibration phase was set with a simulation time of 10 ps and an interval of 2 ps. The Implicit Solvent Model was set to Generalized Born with Simple Switching (GBSW), and the dynamics integrator protocol used LeapfroyVerlet.[32]

4.3.3. Ramachandran Plot. Ramachandran Plot was generated using Discovery Studio 4.0 for both free protein and 4b-eIF4E complex to verify predicted torsion angles in protein during interaction with 4b.

4.3.4. ADMET and Toxicity Studies. Previously prepared structure ligands and reference Ribavirin were subjected to ADMET protocol and toxicity prediction studies with the selection of certain TOPKAT Ames protocols for evaluation.[34]

4.4. Preparation of 4b/Niosomes (4b-NSs). 4b-NSs were generated using a modified thin-film hydration technique.[49] In a molar ratio of (2:1:1), a total of 120 mmol of cholesterol, Span 60, and Tween 60 was used. Briefly, the cholesterol, surfactants, and compound **4b** were all dissolved in chloroform:ethanol:methanol (1:1:1). A Laboratory 4000 rotary evaporator (Heidolph Instruments, Schwabach, Germany) equipped with a vacuum pump (KNF Neuberger GmbH, Freiburg, Germany) was used to evaporate the organic solvent under reduced pressure for 1 h at 60 C, leaving a thin lipid film. The thin film in a rotary evaporator, under normal pressure at 60 °C for 1 h, was dissolved in phosphate buffer saline (pH 7.4). The suspensions were sonicated for 5 min in a bath sonicator (Elma Hans Schmidbauer, Singen, Germany). The prepared suspensions were then left at room temperature for 45 min before being stored at 4 °C for further investigation. Empty niosomes were prepared using the same protocol without adding the drug.

4b-NSs coated with chitosan (Cs/**4b**-NSs) were prepared as previously reported with some modifications.[52] Briefly, 1% chitosan (prepared in acetate buffer solution at pH 4) was added dropwise to an equal volume of **4b**-NSs while being magnetically stirred at 300 rpm and then left at room temperature for 30 min.

4.4.1. Physicochemical Characterization of the Prepared 4b-NSs and Cs/4b-NSs. The average particle size, PDI, and zeta potential were studied by employing a Zetasizer Nano ZS equipped with a 10 mW HeNe laser (Malvern Instruments, Worcestershire, UK). The size measurement was conducted in triplicate at 25 °C. The morphology of Cs/**4b**-NSs was examined utilizing transmission electron microscopy (TEM) (JEOL-JEM 2100 electron microscope, Musashino, Akishima, Tokyo, Japan) operating at 160 kV.

4.4.2. Entrapment Efficiency (EE%). As detailed previously, the EE% of the loaded L1 from **4b**-NSs and Cs/**4b**-NSs was determined by the indirect method with few modifications.[51] Briefly, either **4b**-NSs or Cs/**4b**-NSs were centrifuged at 10,000 rpm and 4 °C for 4 h (Hermle Z 326 K, Labortechnik GmbH, Wehingen, Germany). Then, the supernatant was separated, and the unloaded **4b** was quantified employing ultraviolet−visible (UV−vis) spectroscopy (Cary 500 UV−visible spectrophotometer, Agilent Technologies, California, USA) by measuring absorbance at 250 nm. Equation 1 was used to calculate the EE%.

$$EE\% = \frac{\text{initial amount of drug} - \text{amount of free drug}}{\text{initial amount of drug}} \times 100$$

(1)

4.4.3. In Vitro Release Percentage (%). The *in vitro* release percentage (%) of **4b** from Cs/**4b**-NSs was studied by using the dialysis membrane method. Briefly, a known volume of the niosomes loaded with **4b** was injected into a dialysis bag (cutoff molecular weight of 12−14 kD). The dialysis bag was then positioned into 15 mL of phosphate buffer saline (PBS, pH 7.4 and 5.5) containing fetal bovine serum (0.5%, FBS) and Tween 80 (1.5%) in a shaking incubator (Jeio Tech SI-300, Seoul, Korea), rotating at 350 rpm at 37 °C. At definite

time intervals, a 1 mL aliquot of the sample was withdrawn and immediately replaced with an equal volume of buffer solution. The concentration of released **4b** was detected in the withdrawn aliquot utilizing ultraviolet−visible (UV−vis) spectroscopy (Cary 500 UV−visible spectrophotometer, Agilent Technologies, California, USA) at 250 nm. The release % was computed using eq 2.

$$\text{release \%} = \frac{\text{amount of released \textbf{4b}}}{\text{initial amount of loaded \textbf{4b}}} \times 100 \qquad (2)$$

4.5. *In Vitro* Assays. *4.5.1. Cell Culture and Conditioning.* The cytotoxicity of all compounds was assessed using four different cell lines, namely, hepatocellular carcinoma cells (HepG2), breast carcinoma (MCF-7), colorectal adenocarcinoma (Caco-2), and kidney normal cells (Vero). The culture medium used for all cell lines was RPMI 1640 supplemented with 10% (v/v) heat-inactivated fetal bovine serum (FBS), 100 U/mL penicillin, and 100 μg/mL streptomycin. Cells were seeded in 96-well plates at 10,000 cells/well inoculum density. The cells were kept in a humidified 5% (v/v) CO_2 atmosphere at 37 °C.

The cytotoxic potentials of test compounds were assessed using the SRB assay method as previously described by Skehan et al.[53] The assay simply resides on the notion that the SRB assay is based on the ability of the SRB dye to bind electrostatically and pH-dependently on protein basic amino acid residues. Under mild acidic conditions, SRB binds to protein basic amino acid residues of trichloroacetic acid (TCA)-fixed cells. It can be quantitatively extracted from cells and solubilized for optical density (OD) measurement by weak bases, such as the Tris base.

4.5.2. Measurement of Total Protein Expression. 4.5.2.1. Protein Extraction from Cultured Cells. The culture media were discarded, and the cells' monolayer was washed using ice-cold PBS. PBS was discarded, and 1 mL of ice-cold lysis buffer was added. The cells were scraped using a cold plastic cell scraper and collected in 1.5 mL microcentrifuge tubes, followed by agitation for 30 min at 4 °C. Finally, the tubes were centrifuged at 160,000g for 20 min at 4 °C, the supernatant was collected in a fresh sterile tube to be used for protein extraction, and the cell pellet was discarded.

4.5.2.2. Normalized Total Protein Concentration of Samples. The total protein concentration was measured in the cell lysate using a Coomassie protein assay kit, cat no. 27813 (Sigma-Aldrich, Germany). One hundred microliters of the cell lysate was transferred to a 2 mL centrifuge tube, the Coomassie reagent was added, and the absorbance was measured at 280 nm. Finally, the protein concentration was calculated using the protein standard curve.

4.5.2.3. Preparation of Samples for Loading on SDS-PAGE Gel. Samples were prepared for electrophoresis by an equal volume of loading buffer (2× loading buffer) to the same volume of cell lysate. The mixture was boiled at 95 °C for 5 min and centrifuged at 16,000g for 5 min, and samples were used for electrophoresis or stored at −20 °C.

4.5.2.4. SDS-PAGE: Separation of Proteins Based on Protein Size. Polyacrylamide gels are formed by the reaction of acrylamide and bis-acrylamide (*N,N'*-methylene bis-(acrylamide)), resulting in a highly cross-linked gel matrix. The gel acts as a sieve through which the proteins move in response to an electric field. Proteins contain an overall positive or negative charge; this enables the movement of a protein molecule toward the isoelectric point, at which the molecule has no net charge. By denaturing the proteins and giving them a uniform negative charge, separating them based on their size as they migrate toward the positive electrode is possible.

An 8% SDS gel was prepared and soaked in the tank buffer; 15 μL of the sample buffer was mixed with 15 μL of the sample. The gel comb was removed carefully, and 20 μL of samples was added to each well. The used protein marker ladder is PageRuler Unstained Low Range Protein 1.7 to 40 kDa, cat no. 26632 (Thermo Fisher Scientific, USA). The selection was based on the MW of the target protein (21 kDa) and reference protein (40 kDa). The samples were run at 200 V and 80 mA for 150 min. Once the samples had reached the end of the gel and the ladder was totally separated, the electric current was turned off and the gel was removed from the buffer. The upper glass slide was carefully removed, and the gel was released in a Petri dish containing PBS. After the electrophoresis, the gel was placed in a plastic tray containing a gel-fix solution. The tray was placed on a rocking table and fixed the proteins for 2 h, the gel was fixed in buffer solution, and Coomassie solution was used to stain the gel. The gel was placed on a rocking table and stained for 2−4 h. Following the staining step, the gel was washed several times with excess distilled water, and the gel was destained using a destaining solution. The gel was placed on a rocking table and destained for about 4 h until clear blue bands on a clear background were visible.

For protein transfer, after destaining, the gels were stored in a gel storage solution and photographed as required. For the transformation step, the gel was transferred to a nitrocellulose membrane. The black side of the transfer sandwich was placed on a plate filled with transfer buffer. Two fiber pads, two filter papers, and the nitrocellulose membrane were soaked in transfer buffer. One fiber pad was added on the black side of the transfer sandwich, one filter paper was added to the transfer sandwich, the gel was added carefully, the membrane was added to the gel, the other filter paper was added on the membrane, and then the other fiber pad was added on the filter paper. The other side of the transfer sandwich was closed, and the whole cassette was added to a tank containing the transfer buffer. The transfer process was run at 20 V for 2 and 1/2 h (for transfer confirmation, make sure that the gel no longer contains any bands and is completely clear).

For membrane staining, after the transfer, the membrane was added to glass Petri dishes, 10 mL of blocking buffer was added to the membrane and was left overnight on a rocking platform, and then the blocking buffer was discarded. One milliliter of 10× wash buffer was mixed with 9 mL of distilled water and then 5 μL of the primary antibody "anti-eIF4E antibody" with catalog number E-AB-60650, Elabscience, USA, and anti-phosphorylated-eIF4E antibody with catalog number MBS9604414, My BioSource, USA, and the β-actin Loading Control Antibody was used as reference protein. The antibody concentration of 1:500 was added to the membrane and left overnight on a rocking platform, and then the primary antibody was discarded. The membrane was washed 3 times with 1× washing buffer, followed by the addition of 1 ml of 10× wash buffer mixed with 9 mL of distilled water, then 5 μL of the secondary antibody "Horse Radish Peroxidase (HRP)-conjugated goat anti-rabbit IgG (H+L)" with cat no. 1305936 (Elabscience, USA) was added on the membrane and left overnight on a rocking platform, and then the secondary antibody was discarded. The membrane was washed 3 times

with 1× washing buffer, followed by addition of 10 mL of blocking buffer, and then mixed with 5 μL of the enhanced chemiluminescence (ECL) substrate with catalog number 34075 (Thermo Fisher Scientific, USA), which was added on the membrane and left overnight on a rocking platform, and then the substrate was discarded.

Finally, the membrane was visualized at a wavelength of 340 nm using the UVP Transilluminator gel documentation system, Analytik Jena, USA. The protein ratio was calculated as the ratio of protein concentration relative to the internal control protein (β-actin); the calculation was performed using Analytica Jena software.

■ ASSOCIATED CONTENT

Data Availability Statement

All data in support of the findings of this study are available within the article. The crystallographic human eIF4E-4EBP1 peptide complex is available at https://www.rcsb.org/structure/3U7X and PDB DOI: 10.2210/pdb 3U7X/pdb.

Ⓢ Supporting Information

The Supporting Information is available free of charge at https://pubs.acs.org/doi/10.1021/acsomega.3c02991.

Results of molecular docking studies (Table S1); results of standard dynamic simulations (Table S2); representative raw data for IC$_{50}$ of compound **4b** (Table S3); ^{1}H NMR of compound **1** (Figure S1); ^{13}C NMR of compound **1** (Figure S2); ^{1}H NMR of compound **2** (Figure S3); ^{13}C NMR of compound **2** (Figure S4); mass spectrum of compound **2** (Figure S5); ^{1}H NMR of compound **3a** (Figure S6); ^{13}C NMR of compound **3a** (Figure S7); mass spectrum of compound **3a** (Figure S8); ^{1}H NMR of compound **3b** (Figure S9); ^{13}C NMR of compound **3b** (Figure S10); ^{1}H NMR of compound **3c** (Figure S11); ^{13}C NMR of compound **3c** (Figure S12); IR spectrum of compound **3c** (Figure S13); ^{1}H NMR of compound **3d** (Figure S14); ^{13}C NMR of compound **3d** (Figure S15); ^{1}H NMR of compound **3e** (Figure S16); ^{13}C NMR of compound **3e** (Figure S17); ^{1}H NMR of compound **3f** (Figure S18); ^{13}C NMR of compound **3f** (Figure S19); ^{1}H NMR of compound **4a** (Figure S20); ^{13}C NMR of compound **4a** (Figure S21); mass spectrum of compound **4a** (Figure S22); ^{1}H NMR of compound **4b** (Figure S23); ^{13}C NMR of compound **4b** (Figure S24); IR spectrum of compound **4b** (Figure S25); mass spectrum of compound **4b** (Figure S26); ^{1}H NMR of compound **4c** (Figure S27); ^{13}C NMR of compound **4c** (Figure S28); ^{1}H NMR of compound **4d** (Figure S29); ^{13}C NMR of compound **4d** (Figure S30); ^{1}H NMR of compound **4e** (Figure S31); ^{13}C NMR of compound **4e** (Figure S32); ^{1}H NMR of compound **4f** (Figure S33); ^{13}C NMR of compound **4f** (Figure S34); western blot gel and bands (Figure S35); western blot gel and bands (Figure S36) (PDF)

■ AUTHOR INFORMATION

Corresponding Authors

Sherif Ashraf Fahmy − *Chemistry Department, School of Life and Medical Sciences, University of Hertfordshire Hosted by Global Academic Foundation, Cairo 11835, Egypt;* ⊙ orcid.org/0000-0003-3056-8281; Phone: +201222613344; Email: sheriffahmy@aucegypt.edu, s.fahmy@herts.ac.uk

Iten M. Fawzy − *Department of Pharmaceutical Chemistry, Faculty of Pharmacy, Future University in Egypt, Cairo 11835, Egypt;* Email: iten.mamdouh@fue.edu.eg

Authors

Reem T. Attia − *Department of Pharmacology and Toxicology and Biochemistry, Faculty of Pharmacy, Future University in Egypt, Cairo 11835, Egypt*

Menna A. Ewida − *Department of Pharmaceutical Chemistry, Faculty of Pharmacy, Future University in Egypt, Cairo 11835, Egypt*

Eman Khaled − *Faculty of Pharmacy, Future University in Egypt, Cairo 11835, Egypt*

Complete contact information is available at: https://pubs.acs.org/10.1021/acsomega.3c02991

Notes

The authors declare no competing financial interest.

■ ACKNOWLEDGMENTS

■ REFERENCES

(1) Hanahan, D.; Weinberg, R. A. Hallmarks of cancer: the next generation. *Cell* **2011**, *144* (5), 646−674.

(2) Sonenberg, N.; Hinnebusch, A. G. Regulation of translation initiation in eukaryotes: mechanisms and biological targets. *Cell* **2009**, *136* (4), 731−745.

(3) Braunstein, S.; Karpisheva, K.; Pola, C.; Goldberg, J.; Hochman, T.; Yee, H.; Cangiarella, J.; Arju, R.; Formenti, S. C.; Schneider, R. J. A hypoxia-controlled cap-dependent to cap-independent translation switch in breast cancer. *Mol. Cell* **2007**, *28* (3), 501−512.

(4) Hinnebusch, A. G.; Lorsch, J. R. The mechanism of eukaryotic translation initiation: new insights and challenges. *Cold Spring Harbor Perspect. Biol.* **2012**, *4* (10), a011544.

(5) Ruggero, D. Translational control in cancer etiology. *Cold Spring Harbor Perspect. Biol.* **2013**, *5* (2), No. a012336.

(6) Jia, Y.; Polunovsky, V.; Bitterman, P. B.; Wagner, C. R. Cap-dependent translation initiation factor eIF4E: an emerging anticancer drug target. *Med. Res. Rev.* **2019**, *32* (4), 786−814.

(7) Liwei, R.; Livingstone, M.; Sukarieh, R.; Petroulakis, E.; Gingras, A. C.; Crosby, K.; Smith, B.; Polakiewicz, R. D.; Pelletier, J.; Ferraiuolo, M. A.; Sonenberg, N. Control of eIF4E cellular localization by eIF4E-binding proteins, 4E-BPs. *RNA* **2008**, *14* (7), 1318−1327.

(8) Tang, Y.; et al.et. al Overexpression of p-4EBP1 associates with p-eIF4E and predicts poor prognosis for non-small cell lung cancer patients with resection. *PloS One* **2022**, *17* (6), No. e0265465.

(9) Alabdullah, M. L.; Ahmad, D. A.; Moseley, P.; Madhusudan, S.; Chan, S.; Rakha, E. The mTOR downstream regulator (p-4EBP1) is a novel independent prognostic marker in ovarian cancer. *J. Obstet. Gynaecol.* **2019**, *39* (4), 522−528.

(10) Qin, X.; Jiang, B.; Zhang, Y. 4E-BP1, a multifactor regulated multifunctional protein. *Cell Cycle* **2016**, *15* (6), 781−786.

(11) Musa, J.; et al.et. al Eukaryotic initiation factor 4E-binding protein 1 (4E-BP1): a master regulator of mRNA translation involved in tumorigenesis. *Oncogene* **2016**, *35* (36), 4675−4688.

(12) Batool, A.; Majeed, S. T.; Aashaq, S.; Majeed, R.; Bhat, N. N.; Andrabi, K. I. Eukaryotic initiation factor 4E is a novel effector of mTORC1 signaling pathway in cross talk with Mnk1. *Mol. Cell. Biochem.* **2020**, *465*, 13−26.

(13) Alayev, A.; Holz, M. K. mTOR signaling for biological control and cancer. *J. Cell. Phys.* **2013**, *228* (8), 1658−1664.

(14) Ptushkina, M.; von der Haar, T.; Karim, M. M.; Hughes, J. M. X.; McCarthy, J. E. G. Repressor binding to a dorsal regulatory site traps human eIF4E in a high cap-affinity state. *EMBO J.* **1999**, *18* (14), 4068−4075.

(15) Xie, J.; Merrett, J. E.; Jensen, K. B.; Proud, C. G. The MAP kinase-interacting kinases (MNKs) as targets in oncology. *Expert Opin. Ther. Targets* **2019**, *23* (3), 187−199.

(16) Proud, C. G. Mnks, eIF4E phosphorylation and cancer. *Biochim. Biophys. Acta - Gene Regul. Mech.* **2015**, *1849* (7), 766−773.

(17) Burotto, M.; Chiou, V. L.; Lee, J. M.; Kohn, E. C. The MAPK pathway across different malignancies: a new perspective. *Cancer* **2014**, *120* (22), 3446−3456.

(18) Kentsis, A.; et al.et. al. Further evidence that Ribavirin interacts with eIF4E. *RNA* **2005**, *11* (12), 1762−1766.

(19) Ghosh, B.; et al.et. al. Nontoxic chemical interdiction of the epithelial-to-mesenchymal transition by targeting cap-dependent translation. *ACS Chem. Biol.* **2009**, *4* (5), 367−377.

(20) Lu, C.; Makala, L.; Wu, D.; Cai, Y. Targeting translation: eIF4E as an emerging anticancer drug target. *Expert Rev. Mol. Med.* **2016**, *18*, No. e2.

(21) Wendel, H. G.; et al.et. al. Dissecting eIF4E action in tumorigenesis. *Genes Dev.* **2007**, *21* (24), 3232−3237, DOI: 10.1101/gad.1604407.

(22) Jin, J.; Xiang, W.; Wu, S.; Wang, M.; Xiao, M.; Deng, A. Targeting eIF4E signaling with Ribavirin as a sensitizing strategy for ovarian cancer. *Biochem. Biophys. Res. Commun.* **2019**, *510* (4), 580−586.

(23) Wang, L.; et al.et. al. Design, synthesis and biological evaluation of bromophenol-thiazolylhydrazone hybrids inhibiting the interaction of translation initiation factors eIF4E/eIF4G as multifunctional agents for cancer treatment. *Eur. J. Med. Chem.* **2019**, *177*, 153−170.

(24) Chen, X.; et al.et.al. Structure-guided design, synthesis, and evaluation of guanine-derived inhibitors of the eIF4E mRNA−cap interaction. *J. Med. Chem.* **2012**, *55* (8), 3837−3851.

(25) Moerke, N. J.; et al.et. al. Small-molecule inhibition of the interaction between the translation initiation factors eIF4E and eIF4G. *Cell* **2007**, *128* (2), 257−267.

(26) Li, S.; et al.et. al. Treatment of breast and lung cancer cells with a N-7 benzyl guanosine monophosphate tryptamine phosphoramidate pronucleotide (4Ei-1) results in chemosensitization to gemcitabine and induced eIF4E proteasomal degradation. *Mol. Pharm.* **2019**, *10* (2), 523−531.

(27) Jia, Y.; Chiu, T. L.; Amin, E. A.; Polunovsky, V.; Bitterman, P. B.; Wagner, C. R. Design, synthesis and evaluation of analogs of initiation factor 4E (eIF4E) cap-binding antagonist Bn7-GMP. *Eur. J. Med. Chem.* **2010**, *45* (4), 1304−1313.

(28) Fan, A.; Sharp, P. P. Inhibitors of Eukaryotic Translational Machinery as Therapeutic Agents. *J. Med. Chem.* **2021**, *64* (5), 2436−2465.

(29) Karnik, A. V.; Kamath, S. S. Enantioselective benzoylation of α-amino esters using (S)-1-benzoyl-2-(α-acetoxyethyl) benzimidazole, a chiral benzimidazolide. *J. Org. Chem.* **2007**, *72* (19), 7435−7438.

(30) Ghosh, P.; Park, C.; Peterson, M. S.; Bitterman, P. B.; Polunovsky, V. A.; Wagner, C. R. Synthesis and evaluation of potential inhibitors of eIF4E cap binding to 7-methyl GTP. *Bioorg. Med. Chem. Lett.* **2005**, *15*, 2177−2180.

(31) Siddiqui, N.; Tempel, W.; Nedyalkova, L.; Volpon, L.; Wernimont, A. K.; Osborne, M. J.; Park, H. W.; Borden, K. L. B. Structural insights into the allosteric effects of 4EBP1 on the eukaryotic translation initiation factor eIF4E. *J. Mol. Biol.* **2012**, *415* (5), 781−792.

(32) Hu, Y.; et al. Investigative on the molecular mechanism of licorice flavonoids anti-melanoma by network pharmacology, 3D/2D-QSAR, molecular docking, molecular dynamics simulation. *Front. Chem.* **2022**, *2*, 152.

(33) Volpon, L.; Osborne, M. J.; Topisirovic, I.; Siddiqui, N.; Borden, K. L. Cap-free structure of eIF4E suggests a basis for conformational regulation by its ligands. *EMBO J.* **2006**, *25* (21), 5138−5149.

(34) Ajala, A.; Uzairu, A.; Shallangwa, G. A.; Abechi, S. E. QSAR, simulation techniques, and ADMET/pharmacokinetics assessment of a set of compounds that target MAO-B as anti-Alzheimer agent. *Future J. Pharm. Sci.* **2023**, *9* (1), 4.

(35) Aboeita, N. M.; Fahmy, S. A.; El-Sayed, M. M. H.; Azzazy, H.M.E.-S.; Shoeib, T. Enhanced Anticancer Activity of Nedaplatin Loaded onto Copper Nanoparticles Synthesized Using Red Algae. *Pharmaceutics* **2022**, *14*, 418.

(36) Fahmy, S. A.; et al. PEGylated Chitosan Nanoparticles Encapsulating Ascorbic Acid and Oxaliplatin Exhibit Dramatic Apoptotic Effects against Breast Cancer Cells. *Pharmaceutics* **2022**, *14*, 407.

(37) Azzazy, H.M.E.-S.; Fahmy, S. A.; Mahdy, N. K.; Meselhy, M. R.; Bakowsky, U. Chitosan-Coated PLGA Nanoparticles Loaded with *Peganum harmala* Alkaloids with Promising Antibacterial and Wound Healing Activities. *J. Nanomater.* **2021**, *11*, 2438.

(38) Fahmy, S. A.; et al.et. al. PLGA/PEG Nanoparticles Loaded with Cyclodextrin-*Peganum harmala* Alkaloid Complex and Ascorbic Acid with Promising Antimicrobial Activities. *Pharmaceutics* **2022**, *14*, 142.

(39) Fahmy, S. A.; Ponte, F.; Sicilia, E.; Azzazy, H. M. E.-S. Experimental and Computational Investigations of Carboplatin Supramolecular Complexes. *ACS Omega* **2020**, *5*, 31456−31466.

(40) Fahmy, S. A.; Ponte, F.; Fawzy, I. M.; Sicilia, E.; Azzazy, H.M.E.-S. Betaine host−guest complexation with a calixarene receptor: enhanced in vitro anticancer effect. *RSC Adv.* **2021**, *11*, 24673−24680.

(41) Fahmy, S. A.; et al.et. al. Molecular Engines, Therapeutic Targets, and Challenges in Pediatric Brain Tumors: A Special Emphasis on Hydrogen Sulfide and RNA-Based Nano-Delivery. *Cancers* **2022**, *14*, 5244.

(42) Fahmy, S. A.; Azzazy, H.M.E.-S.; Schaefer, J. Liposome Photosensitizer Formulations for Effective Cancer Photodynamic Therapy. *Pharmaceutics* **2021**, *13*, 1345.

(43) Fahmy, S. A.; et al. Thermosensitive Liposomes Encapsulating Nedaplatin and Picoplatin Demonstrate Enhanced Cytotoxicity against Breast Cancer Cells. *ACS Omega* **2022**, *7* (46), 42115−42125.

(44) Youness, R. A.; Al-Mahallawi, A. M.; Mahmoud, F. H.; Atta, H.; Braoudaki, M.; Fahmy, S. A. Oral Delivery of Psoralidin by Mucoadhesive Surface-Modified Bilosomes Showed Boosted Apoptotic and Necrotic Effects against Breast and Lung Cancer Cells. *Polymers* **2023**, *15*, 1464.

(45) Fahmy, S. A.; Sedky, N. K.; Ramzy, A.; Abdelhady, M. M. M.; Alabrahim, O. A. A.; Shamma, S. N.; Azzazy, H. M. E. S. Green extraction of essential oils from Pistacia lentiscus resins: Encapsulation into Niosomes showed improved preferential cytotoxic and apoptotic effects against breast and ovarian cancer cells. *J. Drug Delivery Sci. Technol.* **2023**, *87*, No. 104820.

(46) Fahmy, S. A.; et al.et. al. Ozonated Olive Oil: Enhanced Cutaneous Delivery via Niosomal Nanovesicles for Melanoma Treatment. *Antioxidants* **2022**, *11*, 1318.

(47) Sedky, N. K.; Abdel-Kader, N. M.; Issa, M. Y.; Abdelhady, M. M. M.; Shamma, S. N.; Bakowsky, U.; Fahmy, S. A. Co-Delivery of Ylang Ylang Oil of *Cananga odorata* and Oxaliplatin Using Intelligent pH-Sensitive Lipid-Based Nanovesicles for the Effective Treatment of Triple-Negative Breast Cancer. *Int. J. Mol. Sci.* **2023**, *24*, 8392.

(48) Rao, K.; et al.et. al. Bergenin loaded gum xanthan stabilized silver nanoparticles suppress synovial inflammation through modulation of the immune response and oxidative stress in adjuvant induced arthritic rats. *J. Mater. Chem. B* **2018**, *6*, 4486−4501.

(49) Li, D.; et al.et. al. Niosomal Nanocarriers for Enhanced Dermal Delivery of Epigallocatechin Gallate for Protection against Oxidative Stress of the Skin. *Pharmaceutics* **2022**, *14* (4), 726.

(50) Imran, M.; et al.et. al. Double-tailed acyl glycoside niosomal nanocarrier for enhanced oral bioavailability of Cefixime. *Artif. Cells Nanomed. Biotechnol.* **2017**, *45*, 1440−1451.

(51) Duse, L.; et al.et.al. Preparation and Characterization of Curcumin Loaded Chitosan Nanoparticles for Photodynamic Therapy. *Phys. Status Solidi A* **2017**, *215*, 1700709.

(52) Wang, W. X.; Gao, J. Q.; Liang, W. Q. Chitosan-coated liposomes for intracellular oligonucleotides delivery: characteristics and cell uptake behavior. *Drug Delivery* **2011**, *18* (3), 208−214.

(53) Skehan, P.; et al.et. al. New colorimetric cytotoxicity assay for anticancer drug screening. *J. NatI. Cancer Inst.* **1990**, *82* (13), 1107−1112.

(54) Carroll, M.; Borden, K. L. B. The oncogene eIF4E: using biochemical insights to target cancer. *J. Interferon Cytokine Res.* **2013**, *33* (5), 227−238.

(55) Graff, J. R.; et al.et. al. Therapeutic suppression of translation initiation factor eIF4E expression reduces tumor growth without toxicity. *J. Clin. Invest.* **2007**, *117* (9), 2638−2648.

(56) Zuberek, J.; et al.et. al. Phosphorylation of eIF4E attenuates its interaction with mRNA 5′ cap analogs by electrostatic repulsion: intein-mediated protein ligation strategy to obtain phosphorylated protein. *RNA* **2003**, *9* (1), 52−61. http://www.rnajournal.org/cgi/doi/10.1261/rna.2133403

(57) McKendrick, L.; Morley, S. J.; Pain, V. M.; Jagus, R.; Joshi, B. Phosphorylation of eukaryotic initiation factor 4E (eIF4E) at Ser209 is not required for protein synthesis in vitro and in vivo. *Eur. J. Biochem.* **2001**, *268* (20), 5375−5385.

(58) Lakhani, C. M. HHS Public Access. *Physiol. Behav.* **2019**, *176* (3), 139−148.

(59) Furic, L.; et al. eIF4E phosphorylation promotes tumorigenesis and is associated with prostate cancer progression. *Proc. Natl. Acad. Sci. U.S.A.* **2010**, *107* (32), 14134−14139.